



ACMAC's PrePrint Repository

Filtering random layering effects in imaging

L. Borcea and F. Gonzalez del Cueto and G. Papanicolaou and C. Tsogka

Original Citation:

Borcea, L. and del Cueto, F. Gonzalez and Papanicolaou, G. and Tsogka, C.
(2010)

Filtering random layering effects in imaging.

Multiscale Modeling & Simulation, 8 (3). pp. 751-781. ISSN 15403459

This version is available at: <http://preprints.acmac.uoc.gr/2/>

Available in ACMAC's PrePrint Repository: September 2011

ACMAC's PrePrint Repository aim is to enable open access to the scholarly output of ACMAC.

FILTERING RANDOM LAYERING EFFECTS IN IMAGING

L. BORCEA[†], F. GONZÁLEZ DEL CUETO[†], G. PAPANICOLAOU[‡], AND C. TSOGKA[§]

Abstract. Objects that are buried deep in heterogeneous media produce faint echoes which are difficult to distinguish from the backscattered field. Sensor array imaging in such media cannot work unless we filter out the backscattered echoes and enhance the coherent arrivals that carry information about the objects that we wish to image. We study such filters for imaging in strongly backscattering, finely layered media. The filters are based on a travel time transformation of the array data, the normal move-out, used frequently in connection with differential semblance velocity estimation in seismic imaging. In a previous paper [10] we showed that the filters can be used to remove coherent signals from strong plane reflectors. In this paper we show theoretically and with extensive numerical simulations that these filters, based on the normal move-out, can also remove the incoherent arrivals in the array data that are due to fine random layering in the medium.

Key words. array imaging, randomly layered media, filtering.

1. Introduction. We consider an inverse problem for the wave equation, where the goal is to estimate or image the compact support \mathcal{S} of scatterers embedded in a heterogeneous medium, using an array A of active sensors that probe it with broadband pulses and record the time traces of the echoes. In smooth media the echoes are due solely to the scatterers in \mathcal{S} and we can image with Kirchhoff migration and its variants [6, 21, 16, 26]. Imaging is more difficult in heterogeneous media, especially when the echoes back-scattered by inhomogeneities overwhelm those coming from \mathcal{S} .

Back-scattering in heterogeneous media may be caused by deterministic structures such as isolated interfaces, and by clutter. The deterministic structures may be known, or they may also be estimated from the array data. Therefore, it is possible to approximate the form of the strong, primary echoes that they produce, and subtract them from the data, thus emphasizing the reflections from \mathcal{S} [22, 28, 29, 10]. The clutter may consist of numerous inhomogeneities that cannot be known or estimated in detail and will, therefore, degrade the image. The challenge is to filter effectively the backscatter from the clutter in the array data, with no prior information about the location of \mathcal{S} .

The coherent interferometric (CINT) imaging method introduced in [12, 13, 15] deals with echoes that are effected by clutter by back-propagating (migrating) to the image region cross-correlations of the time traces, instead of the traces themselves as it is done in Kirchhoff migration. The cross-correlations are over suitable time and sensor offset windows, and they introduce a statistical smoothing in the imaging process at the expense of some blurring in the image. An optimal smoothing can be determined adaptively by varying the support of the windows and optimizing the quality of the resulting image [12]. The smoothing depends on two decoherence parameters that are characteristic of the scattering environment: the decoherence length and frequency. They quantify the loss of coherence of the wave field due to scattering by the inhomogeneities. CINT images effectively in clutter up to ranges that are of the order of one transport mean free path [33, 34]. Beyond such ranges the coherent echoes are too weak to be enhanced by the cross-correlations alone, and the imaging process should be complemented, if possible, by an additional filtering of clutter effects.

In this paper we study filters for dealing with clutter from randomly layered media. They are of interest

[†]Computational and Applied Mathematics, Rice University, MS 134, Houston, TX 77005-1892. (borcea@caam.rice.edu and fcuetto@caam.rice.edu)

[‡]Mathematics, Stanford University, Stanford CA 94305. (papanico@math.stanford.edu)

[§]Applied Mathematics, University of Crete, GR-71409 Heraklion, Greece (tsogka@tem.uoc.gr)

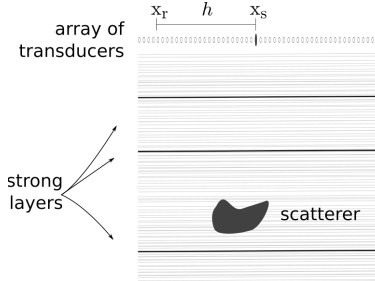


FIG. 2.1. *Schematic of the imaging setup. A compactly supported scatterer is buried in a finely layered medium. The array of transducers lies on the top $z = 0$ and it consists of a source at location $\vec{\mathbf{x}}_s = (\mathbf{x}_s, 0)$ and receivers at points $\vec{\mathbf{x}}_r = (\mathbf{x}_r, 0)$. The medium is finely layered and it may also have some strong scattering interfaces, which we draw with thick black lines.*

because they produce strong backscattering compared to general random media. In particular, they may cause wave localization [36, 34], which means that all of the incident energy is reflected and does not reach beyond a certain depth [36, 2, 30]. The echoes from remote scatterers are overwhelmed by the coda, which are reflections from the random layers. We want to find effective methods to reduce this coda prior to imaging.

We consider data filtering operators \mathbb{Q}_c that annihilate, in principle, the primary echoes that have been scattered once at a strong interface in the medium. This is shown with analysis and numerical simulations in [10]. What is surprising in this work is that the filters \mathbb{Q}_c work better than expected. They also annihilate the incoherent echoes, back-scattered by the fine layers.

In this paper we present a detailed study of filtering with \mathbb{Q}_c of echoes from finely layered media. We show with a detailed analysis and with numerical simulations that the intensity of the layer echoes are reduced significantly by \mathbb{Q}_c , with high probability. The echoes from the compactly supported scatterers are, however, not annihilated by \mathbb{Q}_c , and this is why we can image \mathcal{S} with the filtered data.

The paper is organized as follows: We begin in section 2 with the formulation of the imaging problem and introduce the layer annihilation algorithm. In section 3 we present extensive numerical simulations and assess the performance of the layer annihilation filter \mathbb{Q}_c . The theory is presented in section 4. We end with a summary and conclusions in section 5.

2. Formulation of the imaging problem and the filtering. We consider the array imaging setup shown in Figure 2.1. A finely layered medium occupies the half space $z < 0$ and a scatterer of compact support \mathcal{S} is buried in it. The data are collected at the array \mathcal{A} of N sensors situated on the surface $z = 0$, in the set

$$\mathcal{A} = \left\{ \vec{\mathbf{x}} = (\mathbf{x}, 0), \quad \mathbf{x} \in \mathbb{R}^{d-1}, \quad |\mathbf{x}| \leq \frac{a}{2} \right\}, \quad (2.1)$$

where a is the array aperture. The dimension of the space in (2.1) is $d \geq 2$, and we introduce a coordinate system $\vec{\mathbf{x}} = (\mathbf{x}, z)$ with the origin at the center of the array and with the z axis orthogonal to the layers.

The sensor at $\vec{\mathbf{x}}_s \in \mathcal{A}$ is a source that probes the medium by emitting a short pulse $\vec{\mathbf{F}}(t)$, and the N receivers at $\vec{\mathbf{x}}_r \in \mathcal{A}$ record the echoes (the data). The recordings are time traces of the acoustic pressure field $P(t, \vec{\mathbf{x}}_r; \vec{\mathbf{x}}_s)$, for time t in a window $[t_0, t^*]$, and $r = 1, \dots, N$.

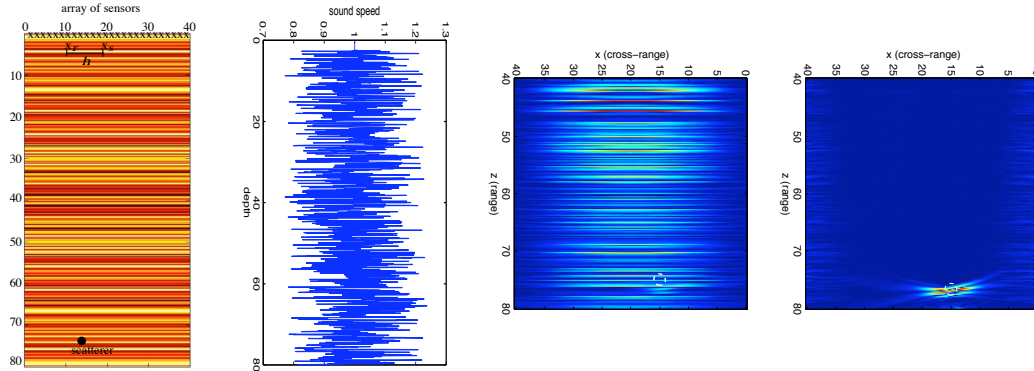


FIG. 2.2. Left two figures: schematic of the problem and the sound speed used in the simulations. The speed is in km/s. The right two figures are migration images computed with functions (2.2) and (2.3), respectively. The abscissa is cross-range in hundreds of meters and the ordinate is depth in hundreds of meters. The small reflector, indicated with the white circle, is obscured by the layers in the first image but it is seen clearly in the right image.

2.1. Migration imaging. Travel time or Kirchhoff migration forms an image at points \vec{y}^s in a search domain $\mathcal{S}^S \supset \mathcal{S}$ by superposing the traces evaluated at the travel times $\tau_c(\vec{x}_r, \vec{y}^s, \vec{x}_s)$.

$$\mathcal{J}^{\text{KM}}(\vec{y}^s) = \sum_{r=1}^N P(\tau_c(\vec{x}_r, \vec{y}^s, \vec{x}_s), \vec{x}_r; \vec{x}_s). \quad (2.2)$$

Migration operates under the assumption that the medium has a smooth and known* sound speed $c(z)$, which determines uniquely the travel times τ_c , by Fermat's principle [8].

In our setup the medium is not smooth because the fine layering produces rapid fluctuations of the wave speed. It is only the background speed $c(z)$ that is smooth or piecewise smooth and known, or at least estimable from the data. The fluctuations cause significant backscattering (i.e., traces with long codas), which impedes the imaging process. The migration function (2.2) has no mechanism for dealing with the coda, so it is not surprising that it does not work well in strong clutter. It gives speckled images that are unreliable and difficult to interpret [11].

Kirchhoff migration may produce useful results for shallow scatterers in finely layered media [14]. This is because of pulse stabilization, which is special to layered media [18, 2, 23, 35, 30]. As the waves propagate through such media they maintain a coherent front which arrives near the travel time τ_c , computed at the background speed $c(z)$. If the coherent echoes from the scatterers in \mathcal{S} are distinguishable from the coda, then we can image them with Kirchhoff migration. However, these scatterers are typically obscured by the fine layering and strong interfaces above them. In particular, the fine layering gives rise to a rapid decay of the amplitude of the coherent front[†] with the depth of \mathcal{S} [18, 30, 23, 35]. The waves loose coherence due to scattering by the finely layered medium, and the array data are typically dominated by the incoherent echoes (i.e., the coda). This is why we cannot image \mathcal{S} with the imaging function (2.2).

Successful imaging of compact scatterers buried deep in layered media requires a preliminary filtering

*If c is not known, then imaging has to be complemented by a velocity estimation, which can be done for example with the semblance approach introduced in [20].

[†]Frequency by frequency, the decay is at an exponential rate, which is faster at the higher frequencies. This is why we observe pulse broadening and amplitude decay.

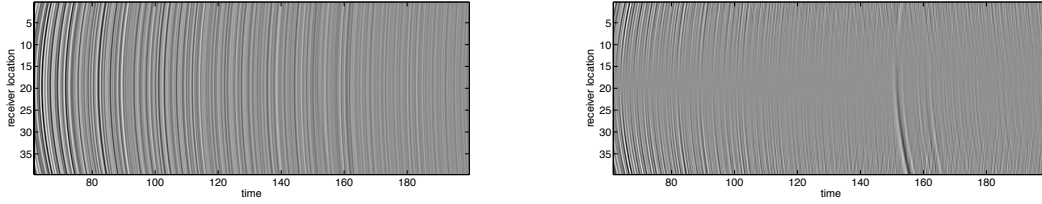


FIG. 2.3. Left: The recorded time traces. Right: The traces after the layer annihilation filtering. The abscissa is time in hundreds of ms and the ordinate is the receiver location on the array, in hundreds of meters.

process, that annihilates the layer echoes and emphasizes the reflections from \mathcal{S} . We introduce below such filters, denoted by \mathbb{Q}_c , and we modify the imaging function as follows

$$\mathcal{J}^{\text{f-KM}}(\vec{\mathbf{y}}^s) = \sum_{r=1}^N \mathbb{Q}_c D(\tau_c(\vec{\mathbf{x}}_r, \vec{\mathbf{y}}^s, \vec{\mathbf{x}}_s), \mathbf{h}_r). \quad (2.3)$$

Here we let

$$D(t, \mathbf{h}_r) = P(t, \vec{\mathbf{x}}_r; \vec{\mathbf{x}}_s), \quad \vec{\mathbf{x}}_r = \vec{\mathbf{x}}_s + (\mathbf{h}_r, 0), \quad (2.4)$$

be the data parametrized by the source-receiver offset \mathbf{h}_r , and we recall that the source is fixed at $\vec{\mathbf{x}}_s \in \mathcal{A}$.

We show in Figure 2.2 the results of a numerical simulation[‡]. The setup is shown in the leftmost figure. We have a small scatterer buried at 7.5km, in a medium with sound speed $v(z)$ shown in Figure 2.2. Because of the fine layering, $v(z)$ has rapid fluctuations around the background speed $c = 1\text{km/s}$. The layers obscure the small scatterer, which cannot be seen in the Kirchhoff migration image (2.2). However, the rightmost image in Figure 2.2 shows that the scatterer is reconstructed well by (2.3), which migrates the filtered data. The traces before and after the filtering are shown in Figure 2.3. Note how the weak echoes from the small scatterer emerge around time 15s in the filtered traces.

2.2. The layer annihilator filters. The layer annihilator filters \mathbb{Q}_c were introduced in [10] with the intention of removing the strong, primary echoes from deterministic interfaces lying above the support \mathcal{S} of the scatterers that we wish to image. By primary reflections we mean the echoes that are scattered once, at an interface in the medium.

DEFINITION 2.1. Consider an arbitrary receiver location $\vec{\mathbf{x}}_r$ in the array, offset by \mathbf{h}_r from the source. Let $\mathcal{N}(\mathbf{h}_r)$ be a neighborhood of source-receiver offsets collinear with \mathbf{h}_r , so that $\mathbf{h}_r \in \mathcal{N}(\mathbf{h}_r)$. Denote by $n(\mathbf{h}_r) \geq 2$ the number of receivers located at $\vec{\mathbf{x}}_{r'} = \vec{\mathbf{x}}_s + (\mathbf{h}_{r'}, 0)$, with $\mathbf{h}_{r'} \in \mathcal{N}(\mathbf{h}_r)$. The filters \mathbb{Q}_c are linear operators that take the data $D(t, \mathbf{h}_r)$ and map it to

$$\mathbb{Q}_c D(t, \mathbf{h}_r) = \left\{ D(T_c(h_r, z), \mathbf{h}_r) - \frac{1}{n(\mathbf{h}_r)} \sum_{\mathbf{h}_{r'} \in \mathcal{N}(\mathbf{h}_r)} D(T_c(h_{r'}, z), \mathbf{h}_{r'}) \right\}_{z=\zeta_c(h_r, t)}. \quad (2.5)$$

Here $h_r = |\mathbf{h}_r|$, $T_c(h_r, z)$ is the arrival time of a primary echo from a presumed interface at depth z , and $\zeta_c(h_r, t)$ is the negative valued, inverse function of $T_c(h_r, z)$, satisfying $T_c(h_r, \zeta_c(h_r, t)) = t$.

[‡]See section 3 for details of the numerical simulation.

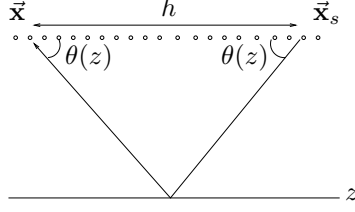


FIG. 2.4. Illustration of scattering at a single interface at depth z .

There are three essential steps in the definition of \mathbb{Q}_c :

Step 1: The mapping of the data from the (t, \mathbf{h}_r) space, to the depth and offset space (z, \mathbf{h}_r) , using the so-called normal move-out [22, 6] map $T_c(h, z)$, given by

$$T_c(h, z) = hK_c + 2 \int_{-|z|}^0 \frac{\sqrt{1 - c^2(z')K_c^2}}{c(z')} dz' = 2 \int_{-|z|}^0 \frac{dz'}{c(z')\sqrt{1 - c^2(z')K_c^2}}, \quad (2.6)$$

Here \mathbf{K}_c is the horizontal slowness vector of plane-like waves reflected at z . It is defined implicitly by Snell's law of reflection

$$\frac{\mathbf{h}}{2} = \mathbf{K}_c \int_{-|z|}^0 \frac{c(z')}{\sqrt{1 - c^2(z')K_c^2}} dz', \quad (2.7)$$

and $K_c = |\mathbf{K}_c|$. Because the right hand side in (2.7) is monotonically increasing with K_c , we have a unique solution which satisfies the identity

$$\mathbf{K}_c = \nabla_{\mathbf{h}} T_c(h, z) = \mathbf{e}_{\mathbf{h}} \frac{d}{dh} T_c(h, z), \quad \mathbf{e}_{\mathbf{h}} = \frac{\mathbf{h}}{h}. \quad (2.8)$$

For example, in the homogeneous case $c(z) = c_o$, equations (2.6)-(2.8) take the explicit form (see Figure 2.4)

$$K_{c_o} = \frac{h}{c_o \sqrt{h^2 + 4z^2}} = \frac{\cos \theta(z)}{c_o}, \quad \text{and} \quad T_{c_o}(h, z) = \frac{\sqrt{h^2 + 4z^2}}{c_o}. \quad (2.9)$$

Step 2: The annihilation step is the subtraction of the local average of the data, after normal move-out. If we had indeed echoes arriving at times $T_c(h_r, z)$, this subtraction would diminish them.

Step 3: In the last step we return to the (t, \mathbf{h}_r) space, using the inverse function $\zeta_c(h_r, t)$. This function exists and it is uniquely defined because $T_c(h_r, z)$ is monotone in z . For example, in the case of constant background speed $c(z) = c_o$, we have $\zeta_{c_o}(h_r, t) = -\frac{\sqrt{c_o^2 t^2 - h_r^2}}{2}$.

REMARK 2.2. *The averaging in (2.5) is confined to a neighborhood $\mathcal{N}(\mathbf{h}_r)$. It is expected that the choice of $\mathcal{N}(\mathbf{h}_r)$ plays a key role in the success of the annihilation. On one hand, the diameter of $\mathcal{N}(\mathbf{h}_r)$ should be much smaller than $|z|$, so that geometrical spreading factors do not play a role in the annihilation. On the other hand, $\mathcal{N}(\mathbf{h}_r)$ should be large enough to contain at least two receivers (i.e., $n(\mathbf{h}_r) \geq 2$), so that the definition makes sense. In practice, we may benefit from dense arrays (i.e., large $n(\mathbf{h}_r)$), because we can also reduce with the averaging in (2.5) additive measurement noise.*

3. Numerical simulations. We present numerical simulations in two dimensions, and refer to a system of coordinates with cross-range axis along the array, in the direction of unit vector \mathbf{e}_1 .

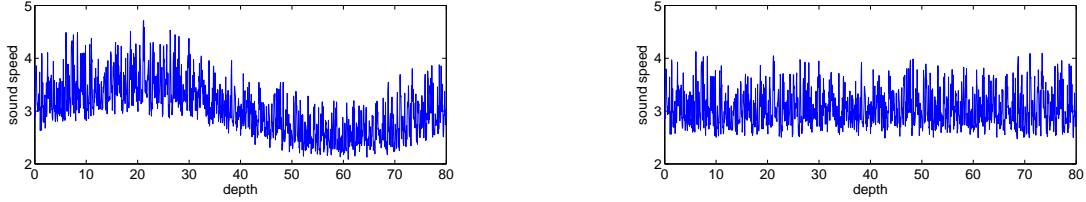


FIG. 3.1. Sound speeds $v(z)$ considered in the numerical simulations. We take three different strengths of the fine scale fluctuations: 13%, 30% and 50%. The plots are for 30% fluctuations. The depth z is in units of $\lambda_o = 100\text{m}$ and the speed is in units of km/s .

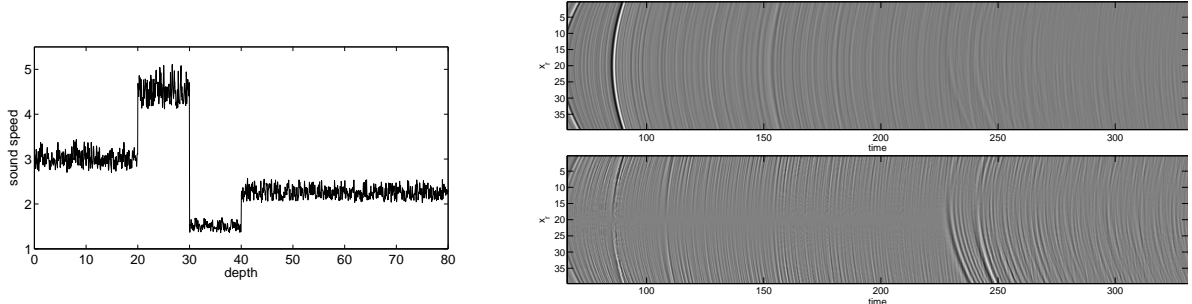


FIG. 3.2. Left: Sound speed $v(z)$ in km/s vs. depth in hundreds of meters. Right: Traces before (top) and after (bottom) annihilation. The abscissa is time scaled by the pulse width of 0.02s . The ordinate is the receiver location in hundreds of meters. The source is at the center of the array and the array is linear of aperture $a = 4\text{km}$.

The array consists of $N = 81$ receivers distributed uniformly, at distance $\lambda_o/2$ apart, in an interval of length $a = 40\lambda_o$, where λ_o is the central wavelength. The source is at the center of the array and it emits downward a pulse given by the derivative of a Gaussian. The pulse width is 0.02s . The central frequency is 30Hz and the bandwidth at 6dB is $20 - 40\text{Hz}$. The sound speed $v(z)$ varies around the scale $c_o = 3\text{km/s}$ (see Figure 3.1). We generate the fine layering using random Fourier series, with Gaussian correlation function and correlation length $\ell = 2\text{m}$. The strength of the fluctuations ranges from 13.3% to 50%. The central wavelength estimated at speed $c_o = 3\text{km/s}$ is $\lambda_o = 100\text{m}$ and the distance from the array to \mathcal{S} is $L \sim 6\text{km}$. We have three acoustic soft scatterers in \mathcal{S} , modeled as disks of radius λ_o , and separated by $2.5\lambda_o$.

We compute the data traces $P(t, \vec{x}_r; \vec{x}_s)$ by solving equations (2.1) with the mixed finite element time domain code ACOUST2D. This code implements the numerical method described in [4] and the finite elements are analyzed in [5]. The infinite extent of the medium is modeled numerically with a perfectly matched absorbing layer surrounding the computational domain [25].

The normal move-out travel times $T_c(h, z)$ are computed from equations (2.6)-(2.7). We use the MATLAB function *fzero* to find the slowness K_c from equation (2.7), and we evaluate the integrals in (2.6)-(2.7) with the MATLAB function *quadl*.

3.1. Annihilation of the echoes from strong scattering interfaces. We begin with an illustration of the annihilation of the echoes from strong scattering interfaces in a medium. We have three deterministic interfaces at depths 2km , 3km and 4km , due to large jump discontinuities of the sound speed $v(z)$, plotted in Figure 3.2. The time traces are shown in the top right picture in Figure 3.2, and they are dominated by the layer echoes. The reflection from the top interface is particularly strong.

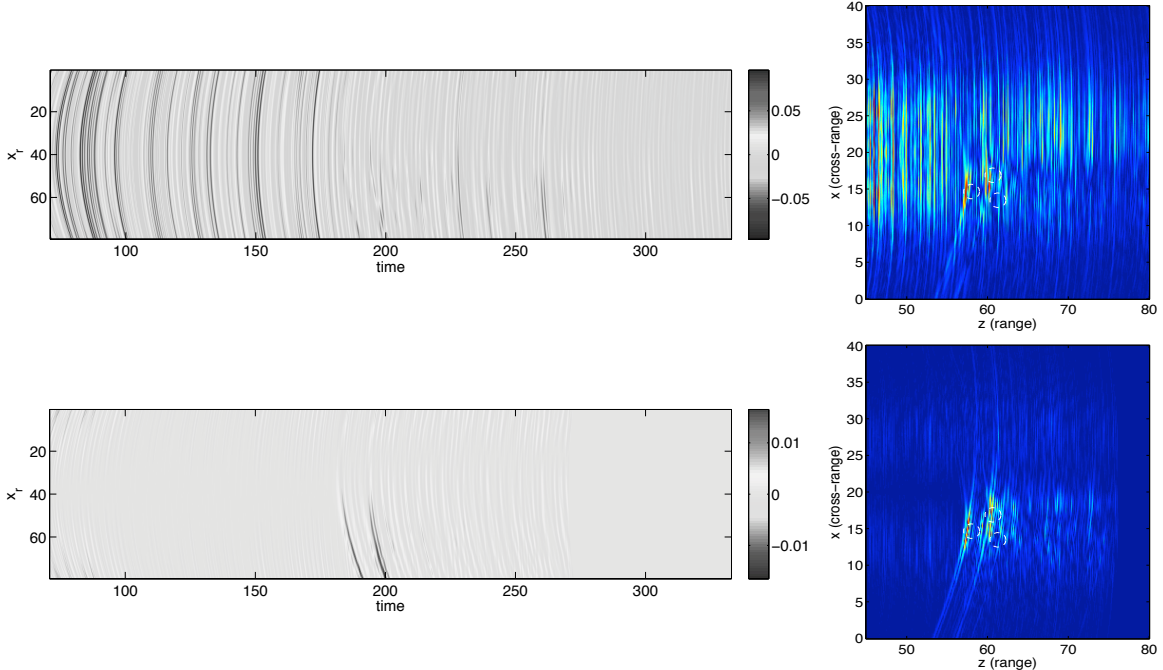


FIG. 3.3. *Top: Data traces in the medium with speed $v(z)$ plotted on the left in Figure 3.1 and the corresponding migration image. Bottom: The annihilated traces and the corresponding migration image. The abscissa in the time traces is time scaled by the pulse width 0.02s, and the ordinate is the receiver location scaled by $\lambda_o = 100\text{m}$. The range and cross-range axes in the images are scaled by λ_o . The scatterers in \mathcal{S} are indicated in the images with white circles.*

The filtered traces are shown in the bottom right plot of Figure 3.2. The filter (2.5) is implemented with

$$\mathcal{N}(\mathbf{h}_r) = \{\mathbf{h}_{r'} = \mathbf{x}_{r'} - \mathbf{x}_s \text{ s.t. } |\mathbf{h}_{r'} - \mathbf{h}_r| \leq \lambda_o/2\}, \quad (3.1)$$

so that $2 \leq n(\mathbf{h}_r) \leq 3$. Note how it annihilates the layer echoes and it emphasizes the reflections from \mathcal{S} , which emerge around time 5s.

3.2. Random layer annihilation. The filter \mathbb{Q}_c annihilates more than the primary echoes from strong interfaces in the medium. It suppresses the random layer echoes too, as seen in Figures 2.3 and 3.2. From now on we focus attention on the random layer annihilation and we suppose that no strong interfaces exist.

We consider first a simulation in the medium with sound speed $v(z)$ plotted on the left in Figure 3.1. The time traces are shown on the left in Figure 3.3. Note the echoes from the compact scatterers emerging in the filtered traces, around time $\tau_c^{\mathcal{S}} \sim 4\text{s}$. These echoes are obscured by the layer reflections in the unfiltered data. The migration images with and without the filtering are shown on the right in Figure 3.3. They are computed with formulas (2.2) and (2.3), respectively. The true location of the scatterers is indicated with white circles in the images in Figure 3.3. Although the scatterers can be seen in the top right picture, the image is noisy due to the layer reflections. The image shown on the bottom right in Figure 3.3 is better. The layer reflections are annihilated by the filter \mathbb{Q}_c and the image is focused on the compact scatterers.

The same conclusion follows from the results shown in Figures 2.2 and 2.3, which are more dramatic, because the support \mathcal{S} is buried deeper in the medium. The scatterer in \mathcal{S} cannot be seen in the migration image in Figure 2.2, but it emerges clearly after the annihilation.

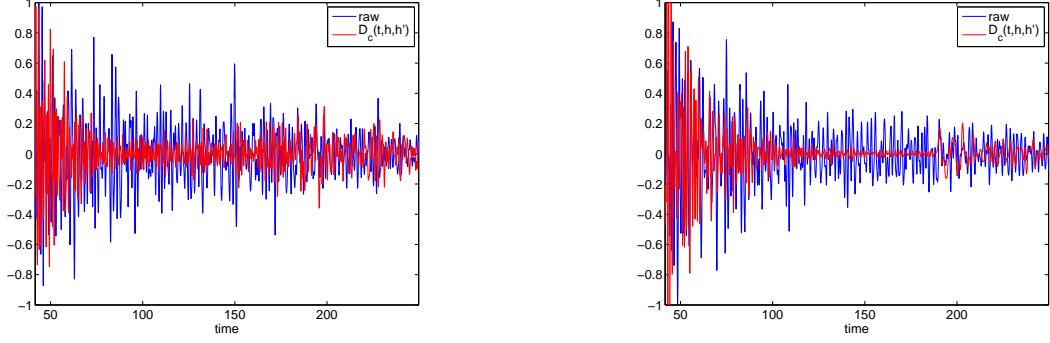


FIG. 3.4. A recorded trace $D(t, \mathbf{h})$ (blue) and the subtracted traces $\mathcal{D}_c(t, \mathbf{h}, \mathbf{h}')$ (red), for offsets $\mathbf{h}' = 15\lambda_o \mathbf{e}_1$ and $\mathbf{h} = \mathbf{0}$. The abscissa is time scaled by the pulse width 0.02s. The background speed is variable on the left and constant on the right. The speeds $v(z)$ are plotted in Figure 3.1. The incoherent echoes are not suppressed in the difference of the two traces, because they are measured at very different offsets.

We study next the behavior of \mathbb{Q}_c for variable and constant mean speeds $c(z)$, and for different strengths of the fluctuations. We also explore numerically how the choice of $\mathcal{N}(\mathbf{h}_r)$ affects the annihilation.

3.2.1. Subtraction of two traces after the normal move-out. Since the layer annihilator averages over the offsets in $\mathcal{N}(\mathbf{h}_r)$ the difference of two traces

$$\mathcal{D}_c(t, \mathbf{h}_r, \mathbf{h}_{r'}) = \{D(T_c(h_r, z), \mathbf{h}_r) - D(T_c(h_{r'}, z), \mathbf{h}_{r'})\}_{z=\zeta_c(h_r, t)},$$

we focus our attention on the study of $\mathcal{D}_c(t, \mathbf{h}, \mathbf{h}')$ in media with constant and variable background speeds $c(z)$. All the results in this section are in the setup of the simulation described above, with three small scatterers buried at depth $L \sim 60\lambda_o$. The realizations of $v(z)$ are shown in Figure 3.1, in the case of 30% strength of the fine scale fluctuations. We also consider weaker and stronger fluctuations of 13% and 50%, respectively.

First, we study the effect of the offset difference $\mathbf{h}' - \mathbf{h}$ on the amplitude of $\mathcal{D}_c(t, \mathbf{h}, \mathbf{h}')$, in the case of 30% fluctuations. Our analysis in section 4.5 will show that we should not get any annihilation if $|\mathbf{h}' - \mathbf{h}| > O(\lambda_o)$, and this is what we observe in Figure 3.4, where $\mathbf{h} = \mathbf{0}$ and $\mathbf{h}' = 15\lambda_o \mathbf{e}_1$. We plot in blue the trace $D(t, \mathbf{0})$, and in red the subtraction of the traces $\mathcal{D}_c(t, \mathbf{0}, 15\lambda_o \mathbf{e}_1)$. The trace $D(t, \mathbf{0})$ is normalized by its maximum amplitude and we use the same normalization constant for the difference of the traces.

Next, we fix the offset difference $\mathbf{h}' - \mathbf{h} = 2.5\lambda_o \mathbf{e}_1$ and we plot in Figure 3.5, with red lines, $\mathcal{D}_c(t, \mathbf{h}, \mathbf{h}')$ for three values of \mathbf{h} : $\mathbf{0}$, $5\lambda_o \mathbf{e}_1$ and $10\lambda_o \mathbf{e}_1$. The fluctuations of $v(z)$ are kept at 30%, as before. We note that the subtraction annihilates the incoherent echoes in both the variable and constant background speed cases. The coherent arrivals around time $t = 4s$ (i.e. 200 pulse widths) are seen in all the red plots in Figure 3.5, but they could not be distinguished in the raw traces shown in blue. The coherent arrivals are weaker in the small offset case, because the scatterers are placed almost beneath the source, and their cross-range is near the unfavorable position[§] $\mathbf{x}_s + \mathbf{h}/2$ described in section 4.6. The coherent arrivals are better seen at the larger offsets $\mathbf{h} = 10\lambda_o \mathbf{e}_1$, but there we have less annihilation at the early times $t = 1s$ (i.e. 50 pulse widths, or penetration depth $\mathcal{L}_t = 15\lambda_o \sim h = 10\lambda_o$).

[§]The traces of the echoes from points with cross-range $\mathbf{x}_s + \mathbf{h}/2$ appear similar to those from a layer, at the source-receiver offset \mathbf{h} .

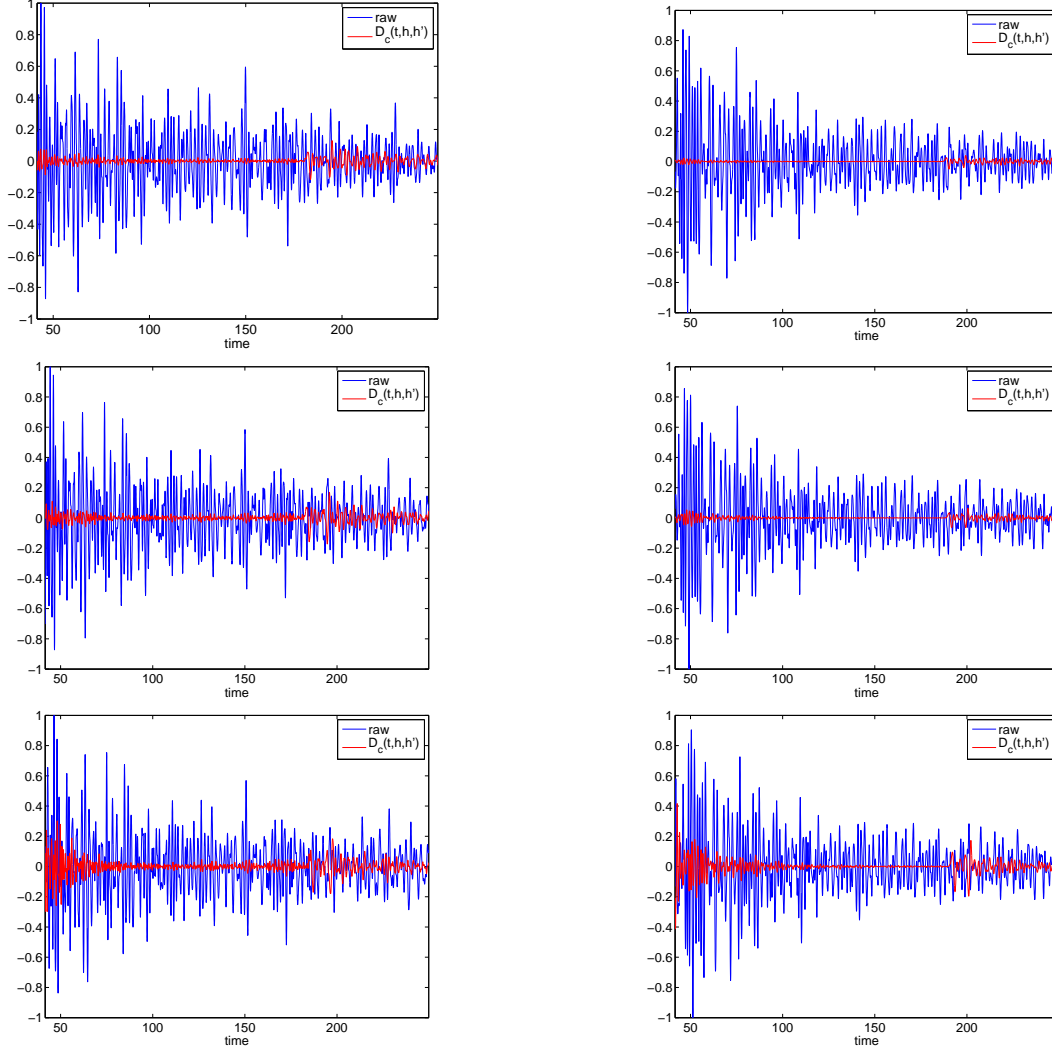


FIG. 3.5. The recorded $D(t, \mathbf{h})$ (blue) and the subtracted traces $\mathcal{D}_c(t, \mathbf{h}, \mathbf{h}')$ (red). The abscissa is time scaled by the pulse width $0.02s$. We have $\mathbf{h}' = \mathbf{h} + 2.5\lambda_0\mathbf{e}_1$, with $\mathbf{h} = \mathbf{0}$ in the top row, $\mathbf{h} = 5\lambda_0\mathbf{e}_1$ in the middle row and $\mathbf{h} = 10\lambda_0\mathbf{e}_1$ in the bottom row. The mean speed is variable on the left column and constant on the right. The speeds $v(z)$ are plotted in Figure 3.1 and the fine scale fluctuations are 30%. The subtraction of the traces annihilates the incoherent echoes from the layers, but not the reflections from S , which emerge around time 200 pulse widths.

Finally, we test the dependence of $\mathcal{D}_c(t, \mathbf{h}, \mathbf{h}')$ on the strength of the fluctuations. We plot in Figure 3.6, with the red line, $\mathcal{D}_c(t, 5\lambda_0\mathbf{e}_1, 7.5\lambda_0\mathbf{e}_1)$ for 13%, and 50% fluctuations. The case of 30% fluctuations is in Figure 3.5. The plots are similar for the constant and variable background speed $c(z)$, so we show only the variable case. We note that the annihilation of the incoherent echoes is almost independent of the strength of the fluctuations. However, the coherent echoes are weaker in the strongly fluctuating media, as expected.

3.3. Velocity estimation based on the annihilation filters. The normal move-out travel time map that enters explicitly in the definition of the filters is determined by the background wave speed $c(z)$. If this is not known, then we must do a velocity estimation. We show here that this can be done in conjunction with the filtering process.

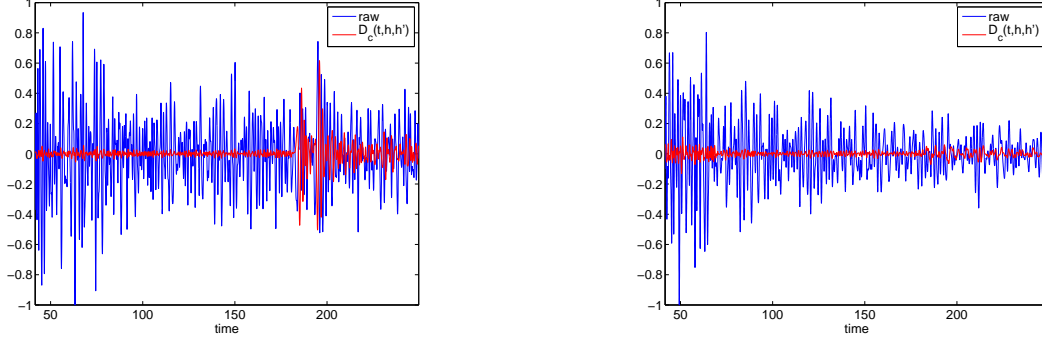


FIG. 3.6. The recorded $D(t, \mathbf{h} = 5\lambda_o \mathbf{e}_1)$ (blue) and the subtracted traces $\mathcal{D}_c(t, \mathbf{h} = 5\lambda_o \mathbf{e}_1, \mathbf{h}' = 7.5\lambda_o \mathbf{e}_1)$ (red). The abscissa is time scaled by the pulse width 0.02s. We have 13% fluctuations of $v(z)$ on the left and 50% on the right. The 30% case is shown in Figure 3.5. The background speed is variable. The realization of $v(z)$ with 30% fluctuations is shown on the left in Figure 3.1.

The estimation of the background speed from random layering reflections has been proposed and analyzed before, in [1, 3, 2]. It requires the approximation of the power spectral density of the echoes, which can be modeled using a special form of transport equations with coefficients dependent on $c(z)$ [1, 3, 2]. It is possible but difficult to approximate the power spectral density with a single realization of the random medium [3, 24]; and new ideas from time reversal bring significant improvements to this process [30]. Nevertheless, the method proposed in [1, 3, 2] remains a complicated task, and our results in this paper suggest that the layer annihilators are a relatively simple alternative for getting approximations of $c(z)$.

To estimate the background speed, we minimize the energy of the annihilated traces over the trial speeds $\tilde{c}(z)$. Since the travel times change with \tilde{c} , it is more convenient to work with the depth coordinate z instead of time, and define the objective function

$$\mathcal{O}(\tilde{c}) = \int_{-\mathcal{L}}^0 dz \sum_{|h_r| \leq \min\{|z|, a/2\}} \left| D(T_c(h_r, z), \mathbf{h}_r) - \frac{1}{n(\mathbf{h}_r)} \sum_{\mathbf{h}_{r'} \in \mathcal{N}(\mathbf{h}_r)} D(T_c(h_{r'}, z), \mathbf{h}_{r'}) \right|^2, \quad (3.2)$$

for a maximum depth $-\mathcal{L}$ dependent on the final observation time. The neighborhood $\mathcal{N}(\mathbf{h}_r)$ is defined in (3.1), and we approximate the z integral with the trapezoidal rule, using a depth sampling in steps of $\lambda_o/10$. We restrict in (3.2) the offsets by $|z|$, because geometrical spreading effects are strong when $h_r > |z|$ and the annihilation is not efficient, as it is based only on arrival times (recall the bottom plots in Figure 3.5).

The unknown $\tilde{c}(z)$ is parametrized by its values at depths $z = -10j\lambda_o$, with $j = 0, 1, \dots$. The field $\tilde{c}(z)$ is the cubic spline interpolation of these values. We optimize first over the depth interval $z \in (-40\lambda_o, 0)$. Then, we fix the speed up to $z = -30\lambda_o$, and we seek in the second step $\tilde{c}(z)$ for $z \in (-60\lambda_o, -30\lambda_o)$. We find that the speeds in the second interval affect very little the objective function. This is to be expected, because the depths in this interval are larger than the array aperture and the traces look flat after the normal move-out, for a wide range of trial speeds. We need a larger aperture to gain sensitivity of the objective function to \tilde{c} at large depths.

We minimize (3.2) with the MATLAB function *fmincon*, and we constrain the trial speeds to the interval $[0.5c_m, 1.5c_M]$, where c_m and c_M are the minimum and maximum values of $c(z)$, respectively. Because of the weak sensitivity of the objective function to the speeds at depths $z \in (-60\lambda_o, -30\lambda_o)$, we regularize

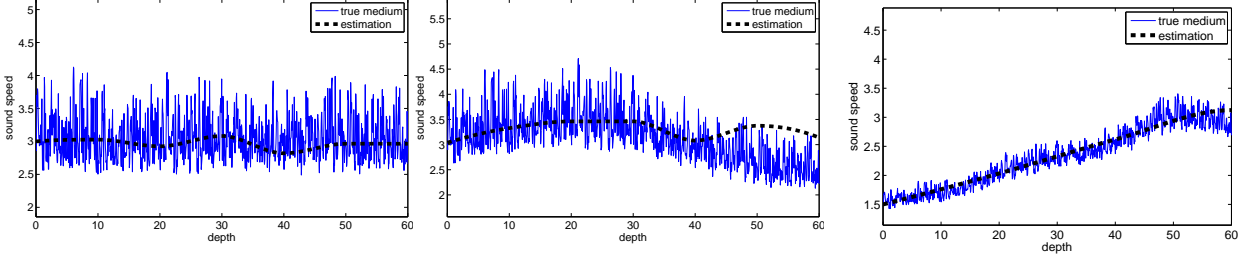


FIG. 3.7. *Velocity estimation results.* We show with the blue solid line the true speed $v(z)$ and with the black dotted line the estimated $c(z)$. The abscissa is negative depth scaled by λ_o and the speed is in units of km/s.

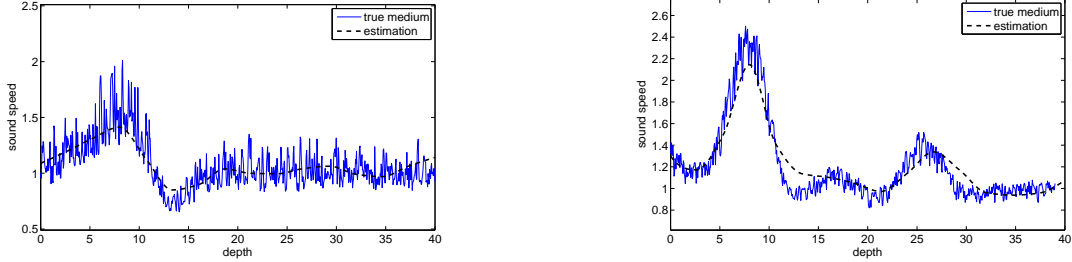


FIG. 3.8. *Velocity estimation in the case of stronger variation of the background speed $c(z)$.* We show with the blue solid line the true speed $v(z)$ and with the black dotted line the estimated $c(z)$. The abscissa is negative depth scaled by λ_o and the speed is in units of km/s.

the second optimization by penalizing the square of the L_2 norm of the gradient of \tilde{c} . The regularization parameter is adjusted to balance the gradient of $\mathcal{O}(\tilde{c})$ with the gradient of the regularization term.

The results shown in Figure 3.7 fit well the actual mean speed, up to depth $z = -40\lambda_o$. We also show in Figure 3.8 the estimated background speeds in media with stronger variations of $c(z)$, for depths above $-40\lambda_o$. Here we took a finer parametrization of $\tilde{c}(z)$, at depths $z = -2.67j\lambda_o$, with $j = 0, 1, \dots, 15$.

4. Analysis. Our goal in the analysis is to give a theoretical explanation of the layer annihilation with the filter \mathbb{Q}_c . We begin with the formulation of the problem in section 4.1 and the mathematical model of the data in section 4.2. Then, we introduce the scaling and the asymptotic regime in section 4.3. The statistics of the incoherent, random layer echoes is described in section 4.4. The proof of the random layer annihilation is in section 4.5.

4.1. Formulation. The mathematical model of the array data is based on the acoustic wave equation in a finely layered medium. The pressure $P(t, \vec{x}; \vec{x}_s)$ satisfies the acoustic wave equations

$$\begin{aligned} \rho \frac{\partial \vec{u}}{\partial t}(t, \vec{x}; \vec{x}_s) + \nabla P(t, \vec{x}; \vec{x}_s) &= \vec{F}(t) \delta(\vec{x} - \vec{x}_s), \\ \frac{1}{V^2(\vec{x})} \frac{\partial P}{\partial t}(t, \vec{x}; \vec{x}_s) + \rho \nabla \cdot \vec{u}(t, \vec{x}; \vec{x}_s) &= 0, \\ \vec{u}(t, \vec{x}; \vec{x}_s) &= \vec{0}, \quad P(t, \vec{x}; \vec{x}_s) = 0, \quad \text{for } t < 0, \end{aligned} \quad (4.1)$$

with excitation from the source at $\vec{x}_s \in \mathcal{A}$ and homogeneous initial conditions. Here \vec{u} is the acoustic velocity and the medium is assumed to have sound speed $V(\vec{x})$ and density ρ . We take constant ρ for simplicity, but

variable densities can be taken into account as shown in [2, 30]. The sound speed $V(\vec{\mathbf{x}})$ satisfies

$$V^{-2}(\vec{\mathbf{x}}) = \begin{cases} v^{-2}(z) + \nu(\vec{\mathbf{x}}) & \text{for } z < 0, \\ c_o^{-2} & \text{for } z \geq 0, \end{cases} \quad (4.2)$$

where we denote by $\nu(\vec{\mathbf{x}})$ the reflectivity of compact support \mathcal{S} , which we wish to estimate, and by $v(z)$ the sound speed in the layered medium. It has a smooth or piecewise smooth part $c(z)$, which determines the travel times, and a rough part that scatters. The smooth part $c(z)$ is either known or can be estimated as was done in Section 3.3. The rough part may consist of strong scattering interfaces due to large jumps of $v(z)$, and of fine layering at a scale $\ell \ll \lambda_o$. The annihilation of the coherent echoes produced by strong interfaces is studied in [10]. Here we are concerned with the annihilation of the waves back-scattered by the finely layered medium, so we assume that no strong interfaces exist. That is to say, we assume that the background speed $c(z)$ is smooth.

Since we cannot know or estimate the fine layering, we model it with a random process

$$v^{-2}(z) = c^{-2}(z) \left[1 + \sigma \mu \left(\frac{z}{\ell} \right) \right], \quad z < 0. \quad (4.3)$$

Here μ is a dimensionless, zero-mean and statistically homogeneous random function of dimensionless argument, which lacks long range correlations. By this we mean that the correlation function $\mathcal{C}(z) = E \{ \mu(0) \mu(z) \}$ decays sufficiently fast at infinity to be integrable over the real line. The process is normalized by $\mathcal{C}(0) = 1$ and $\int_{-\infty}^{\infty} \mathcal{C}(z) dz = 1$, so that

$$\int_{-\infty}^{\infty} E \left\{ \mu(0) \mu \left(\frac{z}{\ell} \right) \right\} dz = \ell, \quad (4.4)$$

with ℓ being the correlation length of the fluctuations. The intensity of the fluctuations is

$$E \left\{ \left[\sigma \mu \left(\frac{z}{\ell} \right) \right]^2 \right\} = \sigma^2, \quad (4.5)$$

and we control it by adjusting the dimensionless parameter $\sigma \leq O(1)$. We cannot have $\sigma \gg 1$ because of the bound constraint $\sigma |\mu(z)| < 1$, for all $z < 0$, which ensures the positivity of the right hand side in (4.3).

At $z = 0$ we take the matching condition $c(0) = c_o$, to avoid a reverberating interface at the surface of the array, and to focus our study on the incoherent wave field back-scattered by the random medium.

4.2. Model of the data. The pressure field $P(t, \vec{\mathbf{x}}_r; \vec{\mathbf{x}}_s)$ recorded at the array consists of two parts: The direct arrival from the source at $\vec{\mathbf{x}}_s$ and the scattered field. The direct arrival carries no information about the medium and it can be removed by tapering the data for $t \leq |\vec{\mathbf{x}}_r - \vec{\mathbf{x}}_s|/c_o$. The scattered field contains the echoes from \mathcal{S} and the unwanted reflections from the layers. The echoes from \mathcal{S} arrive at $t \geq \tau_c^S$, where

$$\tau_c^S = \min_{\vec{\mathbf{y}} \in \mathcal{S}, \vec{\mathbf{x}}_r \in \mathcal{A}} \tau_c(\vec{\mathbf{x}}_s, \vec{\mathbf{y}}, \vec{\mathbf{x}}_r), \quad (4.6)$$

and $\tau_c(\vec{\mathbf{x}}_s, \vec{\mathbf{y}}, \vec{\mathbf{x}}_r)$ are travel times computed at speed $c(z)$, from the source at $\vec{\mathbf{x}}_s \in \mathcal{A}$ to points $\vec{\mathbf{y}} \in \mathcal{S}$, and then back to the array, at $\vec{\mathbf{x}}_r \in \mathcal{A}$. Pulse stabilization [2, 23, 35], which is special to randomly layered media, allows us to use travel times computed with speed $c(z)$ to decide if the waves have reached the scatterer

in \mathcal{S} or not. As they travel through the medium, the waves maintain a coherent front which scatters at points $\vec{\mathbf{y}} \in \mathcal{S}$ and arrives at the array at times $\approx \tau_c(\vec{\mathbf{x}}_s, \vec{\mathbf{y}}, \vec{\mathbf{x}}_r)$. The coherent image formation relies on these coherent echoes, which we model with the Born approximation, as given in Lemma 4.2. The layer reflections are described in Lemma 4.1. It is typical that they dominate the data, and we wish to annihilate them prior to imaging.

LEMMA 4.1. *Let $P^{lay}(t, \vec{\mathbf{x}}_r; \vec{\mathbf{x}}_s)$ be the pressure field back-scattered by the layers in the medium, observed at times $t \in [t_0, t^*]$, with $t_0 > |\vec{\mathbf{x}}_r - \vec{\mathbf{x}}_s|/c_o$. It can be modeled as a superposition of up going plane waves*

$$P^{lay}(t, \vec{\mathbf{x}}_r; \vec{\mathbf{x}}_s) = \frac{1}{2(2\pi)^d} \int d\omega \omega^{d-1} \int d\mathbf{K} \hat{\varphi}(\omega, \mathbf{K}) \mathcal{R}_{t^*}(\omega, K, 0) e^{-i\omega t + i\omega \mathbf{K} \cdot (\mathbf{x}_r - \mathbf{x}_s)}, \quad (4.7)$$

traveling at horizontal slowness \mathbf{K} , and vertical speed $c(K, z) = [c^{-2}(z) - K^2]^{-1/2}$, where $K = |\mathbf{K}|$. The frequencies ω span the bandwidth of the source pulse $\vec{\mathbf{F}}(t) = (\mathbf{f}(t), f(t))$, with Fourier coefficients

$$\left(\hat{\mathbf{f}}(\omega), \hat{f}(\omega) \right) = \int dt (\mathbf{f}(t), f(t)) e^{i\omega t}. \quad (4.8)$$

The amplitudes are modulated by

$$\hat{\varphi}(\omega, \mathbf{K}) = \hat{f}(\omega) - c(K, 0) \mathbf{K} \cdot \hat{\mathbf{f}}(\omega), \quad (4.9)$$

and the random reflection coefficients $\mathcal{R}_{t^*}(\omega, K, z)$ evaluated at the surface of measurements $z = 0$. These coefficients describe the reflections in the strip $[-\mathcal{L}_{t^*}, z] \subseteq [-\mathcal{L}_{t^*}, 0]$, bounded by \mathcal{L}_{t^*} , the maximum depth that influences the array data up to time t^* . They satisfy the Riccati equations

$$\begin{aligned} \frac{\partial}{\partial z} \mathcal{R}_{t^*}(\omega, K, z) &= \frac{-i\omega \sigma \mu (z/\ell) c(K, z)}{2c^2(z)} \left\{ e^{-2i\omega\tau(K, z)} - 2\mathcal{R}_{t^*}(\omega, K, z) + e^{2i\omega\tau(K, z)} [\mathcal{R}_{t^*}(\omega, K, z)]^2 \right\} \\ &\quad + \frac{\partial}{\partial z} \ln \sqrt{c(K, z)} \left\{ e^{-2i\omega\tau(K, z)} - e^{2i\omega\tau(K, z)} [\mathcal{R}_{t^*}(\omega, K, z)]^2 \right\}, \quad z > -\mathcal{L}_{t^*}, \\ \mathcal{R}_{t^*}(\omega, K, -\mathcal{L}_{t^*}) &= 0, \end{aligned} \quad (4.10)$$

with phases determined by the travel times

$$\tau(K, z) = \int_0^z \frac{dz'}{c(K, z')}. \quad (4.11)$$

We refer to Appendix A for the proof of this lemma, and we note that the array data $P(t, \vec{\mathbf{x}}_r; \vec{\mathbf{x}}_s)$ satisfies

$$P(t, \vec{\mathbf{x}}_r; \vec{\mathbf{x}}_s) = P^{lay}(t, \vec{\mathbf{x}}_r; \vec{\mathbf{x}}_s), \quad \text{for } t \in (|\vec{\mathbf{x}}_r - \vec{\mathbf{x}}_s|/c_o, t^*] \text{ and } t^* < \tau_c^{\mathcal{S}}. \quad (4.12)$$

After $\tau_c^{\mathcal{S}}$, the array records the echoes $P^{\mathcal{S}}(t, \vec{\mathbf{x}}_r; \vec{\mathbf{x}}_s)$ from the reflectivity $\nu(\vec{\mathbf{x}})$ supported in \mathcal{S} , as well. We model them with the Born approximation, as stated in the next lemma, proved in Appendix A.

LEMMA 4.2. *The Born approximation of the echoes from \mathcal{S} is given by*

$$P^{\mathcal{S}}(t, \vec{\mathbf{x}}_r; \vec{\mathbf{x}}_s) \approx - \int_{\mathcal{S}} d\vec{\mathbf{y}} \nu(\vec{\mathbf{y}}) \frac{\partial^2 P^i(t, \vec{\mathbf{y}}; \vec{\mathbf{x}}_s)}{\partial t^2} \star_t G(t, \vec{\mathbf{x}}_r, \vec{\mathbf{y}}), \quad (4.13)$$

where \star_t denotes time convolution, $P^i(t, \vec{\mathbf{y}}; \vec{\mathbf{x}}_s)$ is the ‘‘incident’’ pressure field impinging on $\vec{\mathbf{y}} \in \mathcal{S}$, and G is the causal Green’s function of the wave equation in the layered medium. The field $P^i(t, \vec{\mathbf{y}}; \vec{\mathbf{x}}_s)$ at point

$\vec{\mathbf{y}} = (\mathbf{y}, \eta) \in \mathcal{S}$ can be modeled as a superposition of down going plane waves,

$$P^i(t, \vec{\mathbf{y}}; \vec{\mathbf{x}}_s) = -\frac{1}{2(2\pi)^d} \int d\omega \omega^{d-1} \int d\mathbf{K} \hat{\varphi}(\omega, \mathbf{K}) \mathcal{T}(\omega, K, \eta) e^{-i\omega[t+\tau(K, \eta)]+i\omega\mathbf{K}\cdot(\mathbf{y}-\mathbf{x}_s)} + \dots, \quad (4.14)$$

with ballistic (coherent) part determined by the transmission coefficients $\mathcal{T}(\omega, K, \eta)$ of the random medium, from the array surface $z = 0$ to depth η . The weaker, incoherent reverberations from the layers are denoted by "...". The Green's function is similar to (4.14), by reciprocity

$$G(t, \vec{\mathbf{y}}, \vec{\mathbf{x}}_r) = -\frac{1}{2(2\pi)^d} \int d\omega \omega^{d-1} \int d\mathbf{K} \mathcal{T}(\omega, K, \eta) e^{-i\omega[t+\tau(K, \eta)]+i\omega\mathbf{K}\cdot(\mathbf{y}-\mathbf{x}_r)} + \dots \quad (4.15)$$

The coherent part of the echoes described in Lemma 4.2 can be modeled with the O'Doherty Anstey (ODA) theory, as described in [31, 19, 2, 23, 35, 30]. ODA describes the pulse stabilization, which says that as the waves propagate through the random medium, they maintain a coherent front. The arrival time of this front is almost as in a smooth medium with sound speed $c(z)$, except for small random shifts. However, the random medium affects significantly the amplitude and the pulse shape at the front. The amplitude decays as the waves loose coherence at an exponential rate, and the pulse broadens because the effect is more pronounced at the higher end of the frequency spectrum. The energy is transferred by scattering, from the coherent front, to the incoherent, back-scattered field, which becomes the dominant part of the array data and a serious impediment to the imaging process.

4.3. Scaling and the asymptotic regime. We consider a regime typical of applications in exploration geophysics [36], where the waves penetrate to depths $L = 5 - 10\text{km}$ that are much larger than the central wavelength $\lambda_o \sim 100\text{m}$ of the probing pulses. The medium fluctuates on a much shorter scale $\ell = 2 - 3\text{m}$, and the fluctuations can be strong, of order one.

We model the regime with the assumption of separation of scales

$$\frac{\lambda_o}{L} \ll 1, \quad \frac{\ell}{\lambda_o} \ll 1, \quad \sigma = O(1), \quad (4.16)$$

and we let L be the reference $O(1)$ length. The asymptotics is with respect to the dimensionless parameter $\epsilon \ll 1$, introduced by scaling the width of the pulse $\vec{\mathbf{F}}(t)$ emitted from $\vec{\mathbf{x}}_s$, with the reference travel time L/c_o . We redefine $\vec{\mathbf{F}}(t)$ as

$$\vec{\mathbf{F}}(t) = (\mathbf{f}^\epsilon(t), f^\epsilon(t)) = \sqrt{\epsilon} (\mathbf{f}(t/\epsilon), f(t/\epsilon)), \quad (4.17)$$

and we scale its amplitude by $\sqrt{\epsilon}$, to get $O(1)$ incoherent echoes at the array, as shown in section 4.5. The base-band signals $f(t)$, $\mathbf{f}(t)$ have central frequency ω_o and bandwidth B .

In the Fourier domain we have

$$\begin{aligned} \hat{\mathbf{f}}^\epsilon\left(\frac{\omega}{\epsilon}\right) &= \int \mathbf{f}^\epsilon(t) e^{i\frac{\omega}{\epsilon}t} dt = \epsilon^{\frac{3}{2}} \int \mathbf{f}\left(\frac{t}{\epsilon}\right) e^{i\omega\frac{t}{\epsilon}} \frac{dt}{\epsilon} = \epsilon^{\frac{3}{2}} \hat{\mathbf{f}}(\omega), \\ \hat{f}^\epsilon\left(\frac{\omega}{\epsilon}\right) &= \epsilon^{\frac{3}{2}} \hat{f}(\omega), \end{aligned} \quad (4.18)$$

which means that the source (4.17) is supported on the high frequencies

$$\omega^\epsilon = \frac{\omega}{\epsilon} \in \left[\frac{\omega_o}{\epsilon} - \frac{B}{2\epsilon}, \frac{\omega_o}{\epsilon} + \frac{B}{2\epsilon} \right] \cup \left[-\frac{\omega_o}{\epsilon} - \frac{B}{2\epsilon}, -\frac{\omega_o}{\epsilon} + \frac{B}{2\epsilon} \right].$$

This is consistent with (4.16), and we change from now on the notation of the central wavelength to λ_o^ϵ , to emphasize that it is an $O(\epsilon)$ length scale,

$$\frac{\lambda_o^\epsilon}{L} = O(\epsilon) \ll 1. \quad (4.19)$$

We also rename the correlation length ℓ^ϵ , and we assume it is $O(\epsilon^2)$, while keeping the strength of the fluctuations $\sigma = O(1)$. Explicitly, we write

$$\int_{-\infty}^{\infty} E \left\{ \sigma \mu(0) \sigma \mu \left(\frac{z}{\ell^\epsilon} \right) \right\} dz = \ell^\epsilon \sigma^2 = \epsilon^2 l, \quad (4.20)$$

with $l = \sigma^2 \ell^\epsilon / \epsilon^2$ the $O(1)$ rescaled correlation length.

Our model of separation of scales (4.16) is

$$\frac{\ell^\epsilon}{\lambda_o^\epsilon} \sim \frac{\lambda_o^\epsilon}{L} \sim \epsilon \ll 1, \quad \sigma \sim 1, \quad (4.21)$$

and we let the remaining length scale a , the array aperture, be much larger than λ_o^ϵ and independent of ϵ . The filters need such an aperture to make a robust differentiation between the layer echoes and the coherent arrivals from the compact scatterers that we wish to image. Imaging and velocity estimation, with or without layer filtering, require an aperture $a \gg \lambda_o^\epsilon$ [8, 21, 6, 20, 10].

Note that (4.21) is a high frequency regime with respect to the large scale variations in the medium, but it is low frequency with respect to the small scale ℓ^ϵ . Because $\lambda_o^\epsilon \gg \ell^\epsilon$, the waves do not interact strongly with the layers, although they are strong ($\sigma \sim 1$), and the random effects average out over distances of order λ_o^ϵ . However, the back-scattering builds up over the long distances of propagation $L \gg \lambda_o^\epsilon$ considered in (4.21), and it becomes a significant component of the data recorded at the array.

There are other scaling regimes that give significant back-scattering and that can be analyzed [2, 30]. For example, the theory in this paper extends almost identically to the *weakly heterogeneous* regime with $\sigma \ll 1$, $L \gg \lambda_o^\epsilon$, and correlation length similar to λ_o^ϵ . The difference is that in the weakly heterogeneous regime the waves sample more efficiently the small scales, and the asymptotic results depend on the specific autocorrelation function of the random fluctuations [30]. In our regime the waves cannot see the small scales in detail, because $\lambda_o^\epsilon \gg \ell^\epsilon$, and in the limit $\epsilon \rightarrow 0$ the fluctuations take the canonical form of *white noise*, independent of the detailed structure of the random function μ .

4.4. Statistics of the back-scattered field. In our scaling, the model (4.7) of the data (2.4) at offset $\mathbf{h} = \mathbf{x} - \mathbf{x}_s$ from the source becomes

$$D(t, \mathbf{h}) = P(t, \vec{\mathbf{x}}; \vec{\mathbf{x}}_s) = \frac{\epsilon^{\frac{3}{2}}}{2(2\pi)^3} \int \frac{d\omega}{\epsilon} \int d\mathbf{K} \left(\frac{\omega}{\epsilon} \right)^2 \hat{\varphi}(\omega, \mathbf{K}) \mathcal{R}_{t^*}^\epsilon(\omega, K, 0) e^{-i\frac{\omega}{\epsilon}t + i\frac{\omega}{\epsilon}\mathbf{K} \cdot \mathbf{h}}, \quad t \leq t^* < \tau_c^S, \quad (4.22)$$

and the reflection coefficients $\mathcal{R}_{t^*}^\epsilon(\omega, K, z) = \mathcal{R}_{t^*}(\omega/\epsilon, K, z)$ satisfy the Riccati equations

$$\begin{aligned} \frac{\partial}{\partial z} \mathcal{R}_{t^*}^\epsilon(\omega, K, z) &= \frac{-i\omega\mu^\epsilon(z)}{2c(z)\sqrt{1-c^2(z)}K^2} \left\{ e^{-2i\frac{\omega}{\epsilon}\tau(K,z)} - 2\mathcal{R}_{t^*}^\epsilon(\omega, K, z) + e^{2i\frac{\omega}{\epsilon}\tau(K,z)} [\mathcal{R}_{t^*}^\epsilon(\omega, K, z)]^2 \right\} \\ &\quad + \frac{\partial}{\partial z} \ln \sqrt{c(K, z)} \left\{ e^{-2i\frac{\omega}{\epsilon}\tau(K,z)} - e^{2i\frac{\omega}{\epsilon}\tau(K,z)} [\mathcal{R}_{t^*}^\epsilon(\omega, K, z)]^2 \right\}, \quad z > -\mathcal{L}_{t^*}, \\ \mathcal{R}_{t^*}^\epsilon(\omega, K, -\mathcal{L}_{t^*}) &= 0, \end{aligned} \quad (4.23)$$

driven by the random function

$$\mu^\epsilon(z) = \frac{\sigma}{\epsilon} \mu \left(\frac{z}{(\epsilon/\sigma)^2 l} \right). \quad (4.24)$$

The second term in the right hand side of (4.23) can be neglected in the asymptotic analysis of the statistical distribution of the reflected field, because it is rapidly oscillating and it averages out in the limit $\epsilon \rightarrow 0$ [30, Theorem 6.4]. For μ^ϵ we have by the central limit theorem that as $\epsilon \rightarrow 0$,

$$\int_{-\mathcal{L}_{t^*}}^z \mu^\epsilon(z') dz' \rightarrow \sqrt{l} W(z), \quad (4.25)$$

where $W(z)$ is standard Brownian motion and the convergence is weak, in distribution. Thus, the random fluctuations in the medium take the canonical form of *white noise* as $\epsilon \rightarrow 0$, and we can calculate all the limit moments of $\mathcal{R}_{t^*}^\epsilon$ using the white noise (diffusion) limit theorems in [7, 32] and [30, Section 6.5]. Our analysis requires the first and second moments of $\mathcal{R}_{t^*}^\epsilon(\omega, K, 0)$, which we quote directly from [30, 2]:

LEMMA 4.3. *In the limit $\epsilon \rightarrow 0$, the reflection coefficients $\mathcal{R}_{t^*}^\epsilon(\omega, K, z)$ have mean zero and they decorrelate rapidly over ω and K . Explicitly, we have*

$$E \left\{ \mathcal{R}_{t^*}^\epsilon(\omega, K, 0) \overline{\mathcal{R}_{t^*}^\epsilon(\omega', K', 0)} \right\} \rightarrow 0, \quad \text{if } \frac{|\omega - \omega'|}{\omega_o} > O(\epsilon) \text{ or } c_o |K - K'| > O(\epsilon), \quad (4.26)$$

and

$$E \left\{ \mathcal{R}_{t^*}^\epsilon \left(\omega + \frac{\epsilon \tilde{\omega}}{2}, K + \frac{\epsilon \tilde{K}}{2}, 0 \right) \overline{\mathcal{R}_{t^*}^\epsilon \left(\omega - \frac{\epsilon \tilde{\omega}}{2}, K - \frac{\epsilon \tilde{K}}{2}, 0 \right)} \right\} \rightarrow \int_{-\infty}^{\infty} ds \int_{-\infty}^{\infty} d\chi W_1(\omega, K, s, \chi, 0) \exp \left[i\tilde{\omega}(s - K\chi) - i\omega \tilde{K}\chi \right], \quad (4.27)$$

where the bar denotes complex conjugate. The limit in (4.27) depends on the solution of the infinite system of transport equations

$$\frac{\partial W_M}{\partial z} + \frac{2M}{c(z)\sqrt{1-c^2(z)K^2}} \frac{\partial W_M}{\partial s} + \frac{2Mc(z)K}{\sqrt{1-c^2(z)K^2}} \frac{\partial W_M}{\partial \chi} = \frac{M^2}{L_{loc}} (W_{M+1} - 2W_M + W_{M-1}), \quad z > -\mathcal{L}_{t^*},$$

$$W_M(\omega, K, s, \chi, z = -\mathcal{L}_{t^*}) = \delta_{0,M} \delta(s) \delta(\chi), \quad M \in \mathbb{Z}, \quad M \geq 0. \quad (4.28)$$

The solutions $W_M(\omega, K, s, \chi, z)$ determine the $2M$ -th order moments of $\mathcal{R}_{t^*}^\epsilon(\omega, K, z)$, at nearby frequencies and slownesses. Because $\mathcal{R}_{t^*}^\epsilon(\omega, K, -\mathcal{L}_{t^*}) = 0$, we have the initial conditions $W_M(\omega, K, \sigma, \chi, -\mathcal{L}_{t^*}) = 0$ for $M \neq 0$, as denoted by the Kronecker delta symbol $\delta_{0,M}$ in (4.28). The right hand side in (4.28) depends on the localization length [36, 34]

$$L_{loc}(\omega, K, z) = \frac{4c^2(z) [1 - c^2(z)K^2]}{\omega^2 l}, \quad (4.29)$$

which coincides in layered media with the scale of exponential decay of the coherent part of the wave field [36, 2, 30].

It is obvious from (4.22) and Lemma 4.3 that the mean back-scattered field satisfies

$$E \{D(t, \mathbf{h})\} \rightarrow 0, \quad \text{as } \epsilon \rightarrow 0. \quad (4.30)$$

This is why we call $D(t, \mathbf{h})$ incoherent. Its intensity and cross-correlation follow from Lemma 4.3:

LEMMA 4.4. *Let \mathbf{h} and \mathbf{h}' be two source-receiver offsets and suppose that they are collinear and they point in the same direction \mathbf{e}_h . Let also t and t' be two observation times. We have*

$$E \{D(t, \mathbf{h})D(t', \mathbf{h}')\} \rightarrow 0, \quad \text{as } \epsilon \rightarrow 0, \quad (4.31)$$

if $|\mathbf{h} - \mathbf{h}'|/a > O(\epsilon)$, (i.e., $|\mathbf{h} - \mathbf{h}'| \gg \lambda_o^\epsilon$) and/or $|t - t'|/t^* > O(\epsilon)$. For nearby offsets $\mathbf{h}' = \mathbf{h} + \epsilon \boldsymbol{\xi}$ and observation times $t' = t + \epsilon \tilde{t}$, with $t \leq t^*$, we get

$$\lim_{\epsilon \rightarrow 0} E \{D(t, \mathbf{h})D(t + \epsilon \tilde{t}, \mathbf{h} + \epsilon \boldsymbol{\xi})\} = \frac{1}{4(2\pi)^3} \int_{-\infty}^{\infty} d\omega \omega^2 \int_0^{K_{t^*}} dK \frac{K}{h} |\hat{\varphi}(\omega, K \mathbf{e}_1)|^2 W_1(\omega, K, t, h, 0) \cos[\omega(\tilde{t} - K\xi)]. \quad (4.32)$$

Here $\xi = |\boldsymbol{\xi}|$ and the upper bound $K_{t^*} = 1/\max_{z > -L_{t^*}} c(z)$ in the slowness integral ensures that we have propagating plane waves with real and positive vertical speed $c(K, z)$. The intensity of the back-scattered field follows from (4.32), in the case $\tilde{t} = 0$ and $\boldsymbol{\xi} = \mathbf{0}$,

$$\lim_{\epsilon \rightarrow 0} E \{[D(t, \mathbf{h})]^2\} = \frac{1}{4(2\pi)^3} \int_{-\infty}^{\infty} d\omega \omega^2 \int_0^{K_{t^*}} dK \frac{K}{h} |\hat{\varphi}(\omega, K \mathbf{e}_1)|^2 W_1(\omega, K, t, h, 0). \quad (4.33)$$

The solution $W_1(\omega, K, t, z)$ of the transport equations (4.28) is discussed in detail in the next section. For now, it suffices to say that it gives an $O(1)$ intensity (4.33) of the back-scattered field, which decays very slowly in time (i.e., depth). The coherent echoes from \mathcal{S} decay at an exponential rate with depth, and this is why they are easily overwhelmed by the incoherent field.

The proof of Lemma 4.4 is in [2, 30]. We review it briefly in Appendix B.

4.5. The annihilation result. Our goal in this section is to compute the intensity $E \{[\mathbb{Q}_c D(t, \mathbf{h})]^2\}$ of the filtered data and to compare it with $E \{[D(t, \mathbf{h})]^2\}$. We say that the annihilation is successful if

$$\lim_{\epsilon \rightarrow 0} E \{[\mathbb{Q}_c D(t, \mathbf{h})]^2\} \ll \lim_{\epsilon \rightarrow 0} E \{[D(t, \mathbf{h})]^2\}. \quad (4.34)$$

It is sufficient to estimate the intensity $E \{[\mathcal{D}_c(t, \mathbf{h}, \mathbf{h}')^2\}$ of the subtraction of two traces after normal move-out

$$\mathcal{D}_c(t, \mathbf{h}, \mathbf{h}') = \{D(T_c(h, z), \mathbf{h}) - D(T_c(h', z), \mathbf{h}')\}_{z=\zeta_c(h_r, t)}, \quad (4.35)$$

because

$$E \{[\mathbb{Q}_c D(t, \mathbf{h})]^2\} = E \left\{ \left[\frac{1}{n(\mathbf{h})} \sum_{\mathbf{h}' \in \mathcal{N}(\mathbf{h})} \mathcal{D}_c(t, \mathbf{h}, \mathbf{h}') \right]^2 \right\} \leq \frac{1}{n(\mathbf{h})} \sum_{\mathbf{h}' \in \mathcal{N}(\mathbf{h})} E \{[\mathcal{D}_c(t, \mathbf{h}, \mathbf{h}')^2\}. \quad (4.36)$$

We have the following result:

THEOREM 4.5. *We must restrict $\mathcal{N}(\mathbf{h})$ in Definition 2.1 to an $O(\lambda_o^\epsilon)$ vicinity of \mathbf{h} for the annihilation to occur. Let then \mathbf{h}' be an arbitrary offset in $\mathcal{N}(\mathbf{h})$, satisfying by definition $\mathbf{h}' = \mathbf{h} + \epsilon \boldsymbol{\xi}$, with collinear \mathbf{h}*

and ξ . We have

$$\lim_{\epsilon \rightarrow 0} E \left\{ [\mathcal{D}_c(t, \mathbf{h}, \mathbf{h} + \epsilon \boldsymbol{\xi})]^2 \right\} = \frac{1}{2(2\pi)^3} \int_{-\infty}^{\infty} d\omega \omega^2 \int_0^{K_{t^*}} dK \frac{K}{h} |\hat{\varphi}(\omega, K \mathbf{e}_1)|^2 W_1(\omega, K, t, h, 0) \{1 - \cos[\omega \xi (K_c - K)]\}, \quad (4.37)$$

so the success of the annihilation depends on the spread of the support of W_1 around the slowness K_c . In the particular case of constant background speed $c(z) = c_o$, the support is at the slowness K_{c_o} and we get perfect annihilation in the limit,

$$\lim_{\epsilon \rightarrow 0} E \left\{ [\mathcal{D}_{c_o}(t, \mathbf{h}, \mathbf{h} + \epsilon \boldsymbol{\xi})]^2 \right\} = 0, \quad \text{and therefore} \quad \lim_{\epsilon \rightarrow 0} E \left\{ [\mathbb{Q}_{c_o} D(t, \mathbf{h})]^2 \right\} = 0. \quad (4.38)$$

That is to say, the filtered echoes converge to zero in L^2 and in probability. Moreover, we can estimate c_o by minimizing over \tilde{c} the energy after the annihilation

$$\int_{t \leq t^*} dt \int_{|\mathbf{h}| \leq a/2} d\mathbf{h} [\mathbb{Q}_{\tilde{c}} D(t, \mathbf{h})]^2$$

since

$$\lim_{\epsilon \rightarrow 0} E \left\{ [\mathbb{Q}_{\tilde{c}} D(t, \mathbf{h})]^2 \right\} = O(\gamma^2), \quad (4.39)$$

for constant trial speeds satisfying the error bound $\frac{|\tilde{c} - c_o|}{c_o} \leq \gamma \ll 1$.

Proof: That no annihilation occurs when $|\mathbf{h} - \mathbf{h}'| \gg \lambda_o^\xi$, can be seen easily from definition (4.35) and the rapid decorrelation of the incoherent field stated in Lemma 4.4. They give

$$E \left\{ [\mathcal{D}_c(t, \mathbf{h}, \mathbf{h}')^2 \right\} \approx E \left\{ [D(t, \mathbf{h})]^2 \right\} + E \left\{ [D(T_c(h', z), \mathbf{h}')^2 \right\} \Big|_{z=\zeta_c(h, t)}.$$

Take then $\mathbf{h}' = \mathbf{h} + \epsilon \boldsymbol{\xi}$, with collinear $\boldsymbol{\xi}$ and \mathbf{h} , and use equation (2.8) to write

$$T_c(h', z) = T_c(h, z) + \epsilon K_c \xi + O(\epsilon^2), \quad \xi = |\boldsymbol{\xi}|, \quad (4.40)$$

for $z = \zeta_c(h, t)$. We obtain from Lemma 4.4 and the smoothness [¶] of the intensity function (4.33) that

$$\lim_{\epsilon \rightarrow 0} E \left\{ [D(T_c(h, z), \mathbf{h}) - D(T_c(h, z) + \epsilon K_c \xi + O(\epsilon^2), \mathbf{h} + \epsilon \boldsymbol{\xi})]^2 \right\} = \frac{1}{2(2\pi)^3} \int_{-\infty}^{\infty} d\omega \omega^2 \int_0^{K_{t^*}} dK \frac{K}{h} |\hat{\varphi}(\omega, K \mathbf{e}_1)|^2 W_1(\omega, K, T_c(h, z), h, 0) \{1 - \cos[\omega \xi (K_c - K)]\}. \quad (4.41)$$

Equation (4.37) follows by setting $z = \zeta_c(h, t)$, since $T_c(h, \zeta_c(h, t)) = t$, by definition.

To complete the proof, we look at the dependence of $W_1(\omega, K, t, h, 0)$ on the slowness K , using the probabilistic representation of the solution of transport equations (4.28). Let us define $\{m(\mathcal{Z})\}_{\mathcal{Z} \geq \mathcal{Z}_{t^*}}$, a Markov jump process with state space on the positive integers, and with dimensionless depth argument

$$\mathcal{Z}(z) = \int_0^z \frac{dz'}{L_{loc}(\omega, K, z')}, \quad (4.42)$$

[¶]The smoothness of $E \left\{ [D(t, \mathbf{h})]^2 \right\}$ with respect to t and \mathbf{h} , can be inferred from [30, 2] and from the calculation below.

scaled by the localization length $L_{loc}(\omega, K, s)$. Here $z > -\mathcal{L}_{t^*}$ and $\mathcal{Z}_{t^*} = \mathcal{Z}(-\mathcal{L}_{t^*})$. The process $m(\mathcal{Z})$ has an absorbing state at $M = 0$ and it jumps from states $M > 0$ to $M \pm 1$, with equal probability $1/2$. The jumps occur at random depths, with exponential distribution and parameter $2M^2$.

The probabilistic representation of W_1 in terms of $m(\mathcal{Z})$ is in the next lemma. The result follows from Feynman-Kac formula [17] and it is derived in [2, 30]. We review the derivation briefly in Appendix C.

LEMMA 4.6. *The solution $W_1(\omega, K, s, \chi, 0)$ of transport equations (4.28), evaluated at $z = 0$, is given by*

$$W_1(\omega, K, s, \chi, 0) = E_1 \left\{ \delta_{0, m(0)} \delta \left[s - \int_{-\mathcal{L}_{t^*}}^0 \frac{2m(\mathcal{Z}(z'))}{c(z')\sqrt{1-c^2(z')K^2}} dz' \right] \delta \left[\chi - \int_{-\mathcal{L}_{t^*}}^0 \frac{2m(\mathcal{Z}(z'))Kc(z')}{\sqrt{1-c^2(z')K^2}} dz' \right] \right\}, \quad (4.43)$$

This is a conditional expectation and we use the short notation $E_1 \{\cdot\}$ for the condition $m(\mathcal{Z}_{t^}) = 1$.*

Note that $W_1(\omega, K, s, \chi, 0)$ depends on ω^2 through the localization length L_{loc} , and it is supported on the positive χ and s , as stated in Appendix B. Note also that $m(\mathcal{Z})$ must be in the absorbing state 0 when $\mathcal{Z} = 0$ (i.e., $z = 0$), in order to participate in (4.43). The lower bound $-\mathcal{L}_{t^*}$ on z' is due to the causality of the wave equation, which says that we cannot observe any echo scattered below $-\mathcal{L}_{t^*}$. More precisely, (recall (2.6)),

$$t^* \leq 2 \int_{-\mathcal{L}_{t^*}}^0 \frac{dz'}{c(z')\sqrt{1-c^2(z')K^2}}, \quad \text{for all } K \in [0, K_{t^*}].$$

In Theorem 4.5 we need $W_1(\omega, K, s, \chi, 0)$ at $s = t < t^*$, so the first Dirac δ in (4.43) acts on the trajectories $m(\mathcal{Z}(z))$ that are absorbed by state 0 at some depth $z' < 0$. Thus, we may drop $\delta_{0, m(0)}$ in (4.43), and note that W_1 is independent of t^* , as long as we observe it at times $s = t < t^*$.

When the background is homogeneous, (4.43) simplifies to

$$W_1(\omega, K, s, \chi, 0) = E_1 \left\{ \delta \left[s - \frac{2\bar{m}}{c_o\sqrt{1-c_o^2K^2}} \right] \delta \left[\chi - \frac{2\bar{m}Kc_o}{\sqrt{1-c_o^2K^2}} \right] \right\}, \quad (4.44)$$

and it depends on a single random variable

$$\bar{m} = \int_{-\mathcal{L}_{t^*}}^0 m(\mathcal{Z}(z')) dz', \quad (4.45)$$

that can be eliminated from the second Dirac δ to obtain

$$W_1(\omega, K, s, \chi, 0) = E_1 \left\{ \delta \left[s - \frac{2\bar{m}}{c_o\sqrt{1-c_o^2K^2}} \right] \right\} \delta [\chi - Kc_o^2s]. \quad (4.46)$$

Thus, $W_1(\omega, K, t, h, 0)$ is supported on the slowness $K = h/(c_o^2t) = K_{c_o}$, and (4.37) becomes

$$\lim_{\epsilon \rightarrow 0} E \left\{ [\mathcal{D}_c(t, \mathbf{h}, \mathbf{h} + \epsilon \boldsymbol{\xi})]^2 \right\} = \int_{-\infty}^{\infty} d\omega \frac{|\hat{\varphi}(\omega, K_{c_o} \mathbf{e}_1)|^2}{2(2\pi)^3 c_o^4 t^2} \mathcal{W}_1(\omega, K_{c_o}, t) \{1 - \cos[\omega \xi (K_c - K_{c_o})]\}, \quad (4.47)$$

with \mathcal{W}_1 given by (see [2, 30] and Appendix C)

$$\mathcal{W}_1(\omega, K_{c_o}, t) = E_1 \left\{ \delta \left[t - \frac{2\bar{m}}{c_o\sqrt{1-c_o^2K_{c_o}^2}} \right] \right\} = \frac{\omega^2 t}{2c_o\sqrt{1-c_o^2K_{c_o}^2}} \left[2 + \frac{\omega^2 t}{4c_o\sqrt{1-c_o^2K_{c_o}^2}} \right]^{-2}. \quad (4.48)$$

This is assuming that $h < c_o t$, so that K_{c_o} is in the domain of integration (i.e., $K_{c_o} < K_{t^*} = 1/c_o$). If this were not the case, then the intensity before and after annihilation would be zero in the limit.

If $c = c_o$, we get $\lim_{\epsilon \rightarrow 0} E \left\{ [\mathcal{D}_{c_o}(t, \mathbf{h}, \mathbf{h} + \epsilon \boldsymbol{\xi})]^2 \right\} = 0$, and therefore $\lim_{\epsilon \rightarrow 0} E \left\{ [\mathbb{Q}_{c_o} D(t, \mathbf{h})]^2 \right\} = 0$. This L^2 convergence implies by Chebyshev's inequality [17] and by $\lim_{\epsilon \rightarrow 0} E \left\{ \mathbb{Q}_{c_o} D(t, \mathbf{h}) \right\} = 0$, that $\mathbb{Q}_{c_o} D(t, \mathbf{h}) \rightarrow 0$ in probability.

Now let $c \rightsquigarrow \tilde{c} = c_o + O(\gamma c_o)$, and recall from (2.8) that $K_{\tilde{c}}$ changes smoothly with \tilde{c} . We have from (4.47) and the mean value theorem that

$$\lim_{\epsilon \rightarrow 0} E \left\{ [\mathcal{D}_{\tilde{c}}(t, \mathbf{h}, \mathbf{h} + \epsilon \boldsymbol{\xi})]^2 \right\} = O(\gamma^2),$$

as stated in (4.39). \square

REMARK 4.7. *The proof of annihilation in the case $c(z) = c_o$ relies on the simplification (4.46) of the probabilistic representation of $W_1(\omega, K, t, h, 0)$. The result extends to small variations of $c(z)$ around a constant value, as shown below. The general case of variable $c(z)$ is difficult to handle analytically, and the support of $W_1(\omega, K, t, h, 0)$ is not restricted to $K = K_c$ anymore. Still, \mathbb{Q}_c diminishes the layer reflections when $W_1(\omega, K, t, h, 0)$ is concentrated around K_c . The spread in K can be studied numerically, by solving the transport equations (4.28) [1]. It depends on $c(z)$ and it should broaden with time. The key filtering for imaging occurs at times $t \leq \tau_c^S$ that cannot be too long, since the waves do not penetrate beyond the localization length. This is probably why \mathbb{Q}_c remains an effective filter for imaging applications in media with variable $c(z)$, as illustrated with numerical simulations in section 3.*

Now, let us discuss briefly the case of small amplitude variations of $c(z)$,

$$c(z) = c_o + \gamma w(z), \quad (4.49)$$

where $\gamma \ll 1$ and $w(z)$ is a smooth function, bounded independently of γ . We get from Lemma 4.6, after expanding the integrands in series of γ , that

$$W_1(\omega, K, t, h, 0) = E_1 \left\{ \delta \left[t - \int_{-\mathcal{L}_{t^*}}^0 \frac{2m(\mathcal{Z}(z'))}{c(z')\sqrt{1-c^2(z')K^2}} dz' \right] \delta \left[h - Kc_o^2 t - \frac{4\gamma K}{\sqrt{1-c_o^2 K^2}} \times \int_{-\mathcal{L}_{t^*}}^0 m(\mathcal{Z}(z'))w(z') dz' + O(\gamma^2) \right] \right\}. \quad (4.50)$$

Here we used the first Dirac δ to rewrite the leading order term $h - Kc_o^2 t$ in the argument of the second one. Because w is bounded independently of γ , and $m(\mathcal{Z}) \geq 0$, we have

$$\left| \int_{\mathcal{L}_{t^*}}^0 m(\mathcal{Z}(z'))w(z') dz' \right| \leq \int_{-\mathcal{L}_{t^*}}^0 m(\mathcal{Z}(z'))|w(z')| dz' \leq C \int_{-\mathcal{L}_{t^*}}^0 \frac{m(\mathcal{Z}(z'))}{c(z')\sqrt{1-c^2(z')K^2}} dz' = \frac{Ct}{2}, \quad (4.51)$$

with constant C satisfying

$$|w(z)|c(z)\sqrt{1-c^2(z)K^2} \leq C, \quad \text{for all } z \leq 0, \quad K < K_{t^*}.$$

The estimate (4.51) and equation (4.50) show that the support of $W_1(\omega, K, t, h, 0)$ in K is confined to an $O(\gamma)$ neighborhood of

$$K_{c_o} = \frac{h}{c_o^2 t} = K_{c_o + \gamma w} + O(\gamma),$$

and we can bound the intensity of the filtered echoes using (4.36) and (4.37),

$$E \left\{ [\mathbb{Q}_{c_o + \gamma w} D(t, \mathbf{h})]^2 \right\} \leq O(\gamma^2), \quad \text{as } \epsilon \rightarrow 0. \quad (4.52)$$

This bound is conservative, but it shows that the annihilation extends to variable speeds in a smooth manner.

4.6. The coherent echoes after the annihilation. To see why the filters \mathbb{Q}_c are useful in imaging, let us comment briefly on their effect on the coherent echoes arriving from the compact objects that we wish to image. For simplicity, we limit this discussion to the case $c(z) = c_o$.

As explained in section 4.2 and in [10, 30], the coherent echoes from points $\vec{\mathbf{y}} \in \mathcal{S}$ arrive at times $\tau_{c_o}(\vec{\mathbf{x}}_s, \vec{\mathbf{y}}, \vec{\mathbf{x}}_r) [1 + O(\epsilon)]$, where $\vec{\mathbf{y}} = (\mathbf{y}, \eta) \in \mathcal{S}$, $|\eta| \sim L$, and

$$\tau_{c_o}(\vec{\mathbf{x}}_s, \vec{\mathbf{y}}, \vec{\mathbf{x}}_r) \equiv \tau_{c_o}^{ODA}(\mathbf{h}, \vec{\mathbf{y}}) = \frac{1}{c_o} \left[\sqrt{\eta^2 + |\mathbf{x}_s - \mathbf{y}|^2} + \sqrt{\eta^2 + |\mathbf{x}_s + \mathbf{h} - \mathbf{y}|^2} \right].$$

Let φ^{ODA} be the pulse shape of these arrivals and recall from section 4.3 that the pulse width is $O(\epsilon)$. Let also the amplitude of these coherent echoes be comparable to that of the incoherent field, which is $O(1)$ in our scaling. This is the regime where the annihilator filters are expected to be useful.

Theorem 4.5 shows that if we subtract the traces at offsets \mathbf{h} and $\mathbf{h}' = \mathbf{h} + \epsilon \boldsymbol{\xi}$, after the normal move-out, we basically remove the incoherent field for $t \leq \tau_c^S$. However, the coherent echoes are not removed by the subtraction,

$$\begin{aligned} & \left\{ \varphi^{ODA} \left[\frac{T_{c_o}(h + \epsilon \boldsymbol{\xi}, z) - \tau_{c_o}^{ODA}(\mathbf{h} + \epsilon \boldsymbol{\xi}, \vec{\mathbf{y}})(1 + O(\epsilon))}{\epsilon} \right] - \varphi^{ODA} \left[\frac{T_{c_o}(h, z) - \tau_{c_o}^{ODA}(\mathbf{h}, \vec{\mathbf{y}})(1 + O(\epsilon))}{\epsilon} \right] \right\}_{z=\zeta_{c_o}(h,t)} \\ & \approx \xi \left[K_{c_o} - \frac{d}{dh} \tau_{c_o}^{ODA}(\mathbf{h}, \vec{\mathbf{y}}) \right] (\varphi^{ODA})' \left[\frac{t - \tau_{c_o}^{ODA}(\mathbf{h}, \vec{\mathbf{y}})(1 + O(\epsilon))}{\epsilon} \right] = O(1), \end{aligned}$$

because $\tau_{c_o}^{ODA}(\mathbf{h}, \vec{\mathbf{y}})$ and $T_{c_o}(h, z)$ have different dependence on the offset. Explicitly, for observation times $t = \tau_{c_o}^{ODA}(\mathbf{h}, \vec{\mathbf{y}})(1 + O(\epsilon))$ that are in the support of the coherent arrivals, we have

$$\frac{d}{dh} \tau_{c_o}^{ODA}(\mathbf{h}, \vec{\mathbf{y}}) = \frac{d\mathbf{h}}{dh} \cdot \frac{(\mathbf{x}_s + \mathbf{h} - \mathbf{y})}{\sqrt{\eta^2 + |\mathbf{x}_s + \mathbf{h} - \mathbf{y}|^2}} \neq K_{c_o} = \frac{h}{c_o^2 t}$$

in all cases, except the special ones $\mathbf{y} = \mathbf{x}_s + \frac{\mathbf{h}}{2}(1 + O(\epsilon))$.

Thus, the filters are useful in imaging because they annihilate the unwanted incoherent field, but not the “signal” (the echoes from the objects that we wish to image).

5. Summary. Sensor array imaging in strongly back-scattering media is complicated by a serious issue: The coherent echoes from the scatterers that we wish to image are weak and they are difficult to extract from the noise-like time traces recorded at the array. Coherent imaging in strongly back-scattering media does not give useful results, unless we can filter out the unwanted back-scattered echoes.

In this paper we present a theoretical and numerical study of such filters, called layer annihilators, for imaging in strongly back-scattering, finely layered media. They are to our knowledge the first example of filters that deal effectively with back-scattering effects from fine layering.

Finely layered media, modeled by randomly layered media, are interesting because they may be considered as a worse case scenario for imaging with strong clutter. In particular, wave localization [36, 34] that

occurs in randomly layered media even when the wave speed has small amplitude fluctuations [36, 2, 30], makes imaging difficult at depths of the order of the localization length.

The layer annihilator filters considered in this paper are easy to implement, they are computationally inexpensive, and they do not require multiple illuminations. The annihilation process involves commonly used techniques in exploration geophysics, such as normal move-out, gather flattening [6, 21] and semblance velocity estimation[20]. These techniques are based on the single scattering approximation in the medium, and so are the filters. It is therefore remarkable that they can suppress the incoherent echoes produced by random media with strong multiple scattering, as we have shown here with analysis and numerical simulations.

The normal move-out travel time map that enters explicitly in the definition of the filters is determined by the background wave speed. If this is not known, then we must do a velocity estimation. It follows from the analysis in this paper that the velocity estimation can be done in conjunction with the filtering process, at least in the case of constant or nearly constant background speeds. The result seems to extend to more general, variable backgrounds, as we have shown with numerical simulations.

The filters studied in this paper work well, but the layering is hard-wired in their design and it is not clear that they extend to other random media. We are now considering more general filtering approaches [9], which require more data gathered from multiple source illuminations.

Acknowledgments. The work of L. Borcea and F. González del Cueto was partially supported by the Office of Naval Research, under grants N00014-05-1-0699, N00014-09-1-0290 and by the National Science Foundation, grant DMS-0604008. The work of G. Papanicolaou was partially supported by US Army grant W911NF-07-2-0027-1, and AFOSR grant FA9550-08-1-0089. The work of C. Tsogka was partially supported by the European FP7 Marie Curie International Reintegration Grant MIRG-CT-2007-203438.

Appendix A. Proof of Lemmas 4.1 and 4.2. The pressure field $P^{lay}(t, \vec{\mathbf{x}})$ solves the wave equation

$$\begin{aligned} \rho \frac{\partial \vec{\mathbf{u}}}{\partial t}(t, \vec{\mathbf{x}}) + \nabla P^{lay}(t, \vec{\mathbf{x}}) &= \vec{\mathbf{F}}(t) \delta(\vec{\mathbf{x}} - \vec{\mathbf{x}}_s), \\ \frac{1}{v^2(z)} \frac{\partial P^{lay}}{\partial t}(t, \vec{\mathbf{x}}) + \rho \nabla \cdot \vec{\mathbf{u}}(t, \vec{\mathbf{x}}) &= 0, \\ \vec{\mathbf{u}}(t, \vec{\mathbf{x}}) = \vec{\mathbf{0}}, \quad P^{lay}(t, \vec{\mathbf{x}}) &= 0, \quad \text{for } t < 0, \end{aligned} \tag{A.1}$$

in the purely layered medium. Here we suppress for simplicity of notation the fixed source location $\vec{\mathbf{x}}_s$ in the arguments of P^{lay} and $\vec{\mathbf{u}}$. Take the Fourier transform over t and the cross-range variable $\mathbf{x} \in \mathbb{R}^{d-1}$

$$\begin{aligned} \hat{P}^{lay}(\omega, \mathbf{K}, z) &= \int dt \int d\mathbf{x} P^{lay}(t, \mathbf{x}, z) e^{i\omega(t - \mathbf{K} \cdot \mathbf{x})}, \\ (\hat{\mathbf{u}}, \hat{u})(\omega, \mathbf{K}, z) &= \int dt \int d\mathbf{x} \vec{\mathbf{u}}(t, \mathbf{x}, z) e^{i\omega(t - \mathbf{K} \cdot \mathbf{x})}, \quad \vec{\mathbf{u}} = (\mathbf{u}, u), \end{aligned} \tag{A.2}$$

and denote by ω the frequency and by \mathbf{K} the dual variable to \mathbf{x} . It is the horizontal slowness vector of plane waves traveling through the medium at vertical background speed $c(K, z)$, satisfying the identity

$$K^2 + c^{-2}(K, z) = c^{-2}(z).$$

Eliminating $\hat{\mathbf{u}}$ from the equations (A.1)-(A.2), we get the one dimensional problem

$$\begin{aligned} i\omega \left[K^2 - \frac{1}{v^2(z)} \right] \hat{P}^{lay} + \rho \frac{\partial \hat{u}}{\partial z} &= 0, \\ -i\omega \rho \hat{u} + \frac{\partial \hat{P}^{lay}}{\partial z} &= 0, \quad z < 0, \end{aligned} \quad (\text{A.3})$$

and the source excitation translates into jump conditions at $z = 0$,

$$\begin{aligned} \hat{P}^{lay}(\omega, \mathbf{K}, 0^+) - \hat{P}^{lay}(\omega, \mathbf{K}, 0^-) &= \hat{f}(\omega) e^{-i\omega \mathbf{K} \cdot \mathbf{x}_s}, \\ \hat{u}(\omega, \mathbf{K}, 0^+) - \hat{u}(\omega, \mathbf{K}, 0^-) &= \frac{\mathbf{K} \cdot \hat{\mathbf{f}}(\omega)}{\rho} e^{-i\omega \mathbf{K} \cdot \mathbf{x}_s}. \end{aligned} \quad (\text{A.4})$$

We model the up going pressure field recorded at the array, by decomposing further \hat{P}^{lay} and \hat{u} into up and down going waves. Following [30, 2], we write

$$\begin{aligned} \hat{P}^{lay}(\omega, \mathbf{K}, z) &= \frac{\sqrt{\rho c(K, z)}}{2} \left[\hat{\alpha}(\omega, \mathbf{K}, z) e^{i\omega \tau(K, z)} - \hat{\beta}(\omega, \mathbf{K}, z) e^{-i\omega \tau(K, z)} \right], \\ \hat{u}(\omega, \mathbf{K}, z) &= \frac{1}{2\sqrt{\rho c(K, z)}} \left[\hat{\alpha}(\omega, \mathbf{K}, z) e^{i\omega \tau(K, z)} + \hat{\beta}(\omega, \mathbf{K}, z) e^{-i\omega \tau(K, z)} \right], \end{aligned} \quad (\text{A.5})$$

where α and β are random variables quantifying the amplitude of the up and down going plane waves, at frequency ω , depth z and slowness \mathbf{K} . They satisfy a coupled system of stochastic ordinary differential equations for $z < 0$, obtained by substituting (A.5) in (A.3), as given in [30, 2]. The initial conditions

$$\begin{aligned} \alpha(\omega, \mathbf{K}, 0^+) &= \alpha(\omega, \mathbf{K}, 0^-) + \frac{e^{-i\omega \mathbf{K} \cdot \mathbf{x}_s}}{\sqrt{\rho c(K, 0)}} \left[\hat{f}(\omega) + c(K, 0) \mathbf{K} \cdot \hat{\mathbf{f}}(\omega) \right], \\ \beta(\omega, \mathbf{K}, 0^-) &= \frac{e^{-i\omega \mathbf{K} \cdot \mathbf{x}_s}}{\sqrt{\rho c(K, 0)}} \hat{\varphi}(\omega, \mathbf{K}), \end{aligned} \quad (\text{A.6})$$

follow from (A.4), (A.5) and the identity $\beta(\omega, \mathbf{K}, 0^+) = 0$, which says that there are no down going waves above the source, in the homogeneous half space $z > 0$.

Thus, $\beta(\omega, \mathbf{K}, 0^-)$ is the down going field emitted by the source at $\vec{\mathbf{x}}_s$. The up going field $\alpha(\omega, \mathbf{K}, 0^+)$ consists of two parts: The direct arrival that has no information about the medium, and the reflected $\alpha(\omega, \mathbf{K}, 0^-)$, that defines the back-scattered field at the array. The amplitude of this field is written in (4.7) as

$$\alpha(\omega, \mathbf{K}, 0^-) = \mathcal{R}_{t^*}(\omega, K, 0) \beta(\omega, \mathbf{K}, 0^-), \quad (\text{A.7})$$

using the reflection coefficient

$$\mathcal{R}_{t^*}(\omega, K, z) = \frac{\alpha(\omega, \mathbf{K}, z)}{\beta(\omega, \mathbf{K}, z)} \quad (\text{A.8})$$

of the medium above depth $-\mathcal{L}_{t^*}$. This reflection coefficient satisfies the Riccati equation (4.10), obtained by substitution of definitions (A.8) and (A.5) in equation (A.3), as given in [30, 2]. The initial condition $\mathcal{R}_{t^*}(\omega, K, -\mathcal{L}_{t^*}) = 0$ follows from

$$\alpha(\omega, \mathbf{K}, -\mathcal{L}_{t^*}) = 0, \quad (\text{A.9})$$

since we cannot observe echoes from depths larger than \mathcal{L}_{t^*} at times $t \leq t^*$. This completes the proof of Lemma 4.1.

To prove Lemma 4.2, it remains to write the ballistic, down going part of the incident field impinging on the scatterer at point $\vec{\mathbf{y}} = (\mathbf{y}, \eta) \in \mathcal{S}$. It is determined by the transmission coefficient $\mathcal{T}(\omega, K, \eta)$, and we write its amplitude in (4.14) as

$$\beta(\omega, K, \eta) = \beta(\omega, K, 0^-) \mathcal{T}(\omega, K, \eta). \quad \square$$

Appendix B. Proof of Lemma 4.4. The proof is summarized from [2, 30]. We begin with expression (4.22) of the data, which we rewrite in polar coordinates

$$D(t, \mathbf{h}) = \frac{1}{2(2\pi)^3 \epsilon^{3/2}} \int_{-\infty}^{\infty} d\omega \int_0^{K_{t^*}} dK \omega^2 K \int_0^{2\pi} d\theta \hat{\varphi}(\omega, K \boldsymbol{\vartheta}_\theta) \mathcal{R}_{t^*}^\epsilon(\omega, K, 0) e^{-i\frac{\omega}{\epsilon} t + i\frac{\omega}{\epsilon} K h \cos \theta}, \quad (\text{B.1})$$

with angle θ measured with respect to the direction of \mathbf{h} and $\hat{\boldsymbol{\vartheta}}_\theta = (\cos \theta, \sin \theta)$. Note that $\hat{\boldsymbol{\vartheta}}_0 = \mathbf{e}_1$.

Recall from Lemma 4.3 the rapid decorrelation of $\mathcal{R}_{t^*}^\epsilon$ over ω and K , and assume a smooth pulse shape $\hat{\varphi}$, to get

$$\begin{aligned} E \{D(t, \mathbf{h}) D(t', \mathbf{h}')\} &= \frac{1}{4(2\pi)^6 \epsilon} \int_{-\infty}^{\infty} d\omega \int_0^{K_{t^*}} dK \omega^4 K^2 \int_{-\infty}^{\infty} d\tilde{\omega} \int_{-\infty}^{\infty} d\tilde{K} E \left\{ \mathcal{R}_{t^*}^\epsilon \left(\omega + \frac{\epsilon \tilde{\omega}}{2}, K + \frac{\epsilon \tilde{K}}{2}, 0 \right) \right. \\ &\quad \left. \overline{\mathcal{R}_{t^*}^\epsilon \left(\omega - \frac{\epsilon \tilde{\omega}}{2}, K - \frac{\epsilon \tilde{K}}{2}, 0 \right)} \right\} \int_0^{2\pi} d\theta \hat{\varphi}(\omega, K \boldsymbol{\vartheta}_\theta) \int_0^{2\pi} d\theta' \overline{\hat{\varphi}(\omega, K \boldsymbol{\vartheta}_{\theta'})} \exp \left\{ -i\frac{\omega}{\epsilon} (t - t') \right. \\ &\quad \left. + i\frac{\omega}{\epsilon} K (h \cos \theta - h' \cos \theta') + i(\omega \tilde{K} + \tilde{\omega} K) \frac{(h \cos \theta + h' \cos \theta')}{2} - i\tilde{\omega} \frac{(t + t')}{2} \right\} + \dots, \end{aligned}$$

where we denote by “...” the lower order terms.

We deal first with the $O(1/\epsilon)$ phase, and then take the limit (4.27). The fast phase depends on the variables $\omega, K, \theta, \theta'$ and the leading order contribution comes from the vicinity of the stationary points satisfying equations

$$\begin{aligned} t - t' - K(h \cos \theta - h' \cos \theta') &= 0, \\ \omega (h \cos \theta - h' \cos \theta') &= 0, \\ \omega K h \sin \theta = \omega K h' \sin \theta' &= 0. \end{aligned}$$

It is easy to see that if $|t - t'|/t^* > O(\epsilon)$, then the only stationary point arises at $\omega = 0$, and it makes no contribution because of the amplitude factor ω^4 . Similarly, if $|t - t'|/t^* \leq O(\epsilon)$, but $|h - h'|/a > O(\epsilon)$, the stationary point is at $\omega = 0$ and $K = 0$, and it makes no contribution, because of the amplitude factor $\omega^4 K^2$. Thus, $E \{D(t, \mathbf{h}) D(t', \mathbf{h}')\}$ is small for $|\mathbf{h} - \mathbf{h}'|/a > O(\epsilon)$ and/or $|t - t'|/t^* > O(\epsilon)$ and it tends to zero as $\epsilon \rightarrow 0$.

Let then $\mathbf{h}' = \mathbf{h} + \epsilon \boldsymbol{\xi}$, $t' = t + \epsilon \tilde{t}$, and observe that now we have stationary points for $\theta = \theta' = 0$ or π ,

with no restriction on ω and K . Integrating over θ and θ' , we obtain

$$E \{D(t, \mathbf{h})D(t + \epsilon \tilde{t}, \mathbf{h} + \epsilon \boldsymbol{\xi})\} = \frac{1}{4(2\pi)^5} \int_{-\infty}^{\infty} d\omega \int_o^{K_{t^*}} dK |\omega|^3 \frac{K}{h} \sum_{q=\pm 1} |\hat{\varphi}(\omega, qK\boldsymbol{\vartheta}_0)|^2 \int_{-\infty}^{\infty} d\tilde{\omega} \int_{-\infty}^{\infty} d\tilde{K}$$

$$E \left\{ \mathcal{R}_{t^*}^\epsilon \left(\omega + \frac{\epsilon \tilde{\omega}}{2}, K + \frac{\epsilon \tilde{K}}{2}, 0 \right) \overline{\mathcal{R}_{t^*}^\epsilon \left(\omega - \frac{\epsilon \tilde{\omega}}{2}, K - \frac{\epsilon \tilde{K}}{2}, 0 \right)} \right\} e^{i\omega[\tilde{t}-qK\xi] + i(\omega\tilde{K} + \tilde{\omega}K)qh - i\tilde{\omega}t} + \dots$$

Next, we use Lemma 4.3 for the limit $\epsilon \rightarrow 0$ of $E \{ \mathcal{R}_{t^*}^\epsilon \overline{\mathcal{R}_{t^*}^\epsilon} \}$,

$$\lim_{\epsilon \rightarrow 0} E \{D(t, \mathbf{h})D(t + \epsilon \tilde{t}, \mathbf{h} + \epsilon \boldsymbol{\xi})\} = \frac{1}{4(2\pi)^5} \int_{-\infty}^{\infty} d\omega \int_o^{K_{t^*}} dK |\omega|^3 \frac{K}{h} \sum_{q=\pm 1} |\hat{\varphi}(\omega, qK\boldsymbol{\vartheta}_0)|^2 e^{i\omega[\tilde{t}-qK\xi]} \int_{-\infty}^{\infty} d\tilde{\omega}$$

$$\int_{-\infty}^{\infty} d\tilde{K} \int_{-\infty}^{\infty} ds \int_{-\infty}^{\infty} d\chi W_1(\omega, K, s, \chi, 0) \exp \left\{ i\tilde{\omega}(s - K\chi) - i\omega\tilde{K}\chi + i(\omega\tilde{K} + \tilde{\omega}K)qh - i\tilde{\omega}t \right\}$$

and we integrate over $\tilde{\omega}$ and \tilde{K} to get

$$\lim_{\epsilon \rightarrow 0} E \{D(t, \mathbf{h})D(t + \epsilon \tilde{t}, \mathbf{h} + \epsilon \boldsymbol{\xi})\} = \frac{1}{4(2\pi)^3} \int_{-\infty}^{\infty} d\omega |\omega|^3 \int_o^{K_{t^*}} dK \frac{K}{h} \sum_{q=\pm 1} |\hat{\varphi}(\omega, qK\boldsymbol{\vartheta}_0)|^2 e^{i\omega(\tilde{t}-qK\xi)}$$

$$\int_{-\infty}^{\infty} ds \int_{-\infty}^{\infty} d\chi W_1(\omega, K, s, \chi, 0) \delta[s - t + K(qh - \chi)] \delta[\omega(qh - \chi)].$$

It turns out (see section 4.5) that $W_1(\omega, K, s, \chi, 0)$ is even in ω and that it is supported on $\chi > 0$, so only $q = 1$ contributes in the sum. The result (4.32) follows from the properties of Dirac δ distributions. \square

Appendix C. Probabilistic representation of the transport equations. We review briefly, from [2, 30], the probabilistic representation of the solution of the transport equations (4.28).

Let us begin with the change of variables (4.42), and remark that $\mathcal{Z}(z)$ is a monotonically increasing function of z . Thus, we may define the inverse map $z = g(\mathcal{Z})$, satisfying

$$g(\mathcal{Z}(z)) = z, \quad \frac{dg(\mathcal{Z})}{d\mathcal{Z}} = L_{loc}(\omega, K, g(\mathcal{Z})), \quad (\text{C.1})$$

and we let

$$c_g(\mathcal{Z}) = [c \circ g](\mathcal{Z}) = c(g(\mathcal{Z})). \quad (\text{C.2})$$

The transport equations (4.28) become

$$\frac{\partial W_M}{\partial \mathcal{Z}} + 2M \left[\frac{L_{loc}}{c_g \sqrt{1 - c_g^2 K^2}} \frac{\partial W_M}{\partial s} + \frac{L_{loc} c_g K}{\sqrt{1 - c_g^2 K^2}} \frac{\partial W_M}{\partial \chi} \right] = M^2 (W_{M+1} - 2W_M + W_{M-1}), \quad \mathcal{Z} > \mathcal{Z}_{t^*},$$

$$W_M = \delta_{0,M} \delta(s) \delta(\chi), \quad \mathcal{Z} = \mathcal{Z}_{t^*}, \quad (\text{C.3})$$

and we wish to solve them using the Markov jump process $\{m(\mathcal{Z})\}_{\mathcal{Z} \geq \mathcal{Z}_{t^*}}$ defined in section 4.5.

To compute the infinitesimal generator \mathbb{G} of the jump process,

$$\mathbb{G}\psi(M) = \lim_{\eta \rightarrow 0} \frac{1}{\eta} [E \{ \psi(m(\mathcal{Z} + \eta)) | m(\mathcal{Z}) = M \} - \psi(M)],$$

we recall the following basic facts: (1) The jump times must be exponentially distributed for the process to be Markovian [27, section XVII.6]. In our case we let $2M^2$ be the parameter in the exponential distribution of the jump times, from state $M > 0$. (2) The probability that we have one jump in the interval $[\mathcal{Z}, \mathcal{Z} + \eta]$ is $2M^2\eta + o(\eta)$, as shown in [27, section XVII.2]. The jump is to $M \pm 1$ with equal probability $1/2$, by definition of the process. (3) The probability of more jumps is $o(\eta)$ and the probability of no jump is $e^{-2M^2\eta} = 1 - 2M^2\eta + o(\eta)$. Using these facts in the definition of \mathbb{G} , we obtain

$$\begin{aligned}\mathbb{G}\psi(M) &= \lim_{\eta \rightarrow 0} \frac{1}{\eta} [\psi(M+1)M^2\eta + \psi(M-1)M^2\eta + \psi(M)(1 - 2M^2\eta) + o(\eta) - \psi(M)] \\ &= M^2 [\psi(M+1) - 2\psi(M) + \psi(M-1)].\end{aligned}\quad (\text{C.4})$$

Now define

$$S(\mathcal{Z}) = s - \int_{\mathcal{Z}_{t^*}}^{\mathcal{Z}} \frac{2mL_{loc}}{c_g\sqrt{1-c_g^2K^2}} d\mathcal{Z}' \quad \text{and} \quad X(\mathcal{Z}) = \chi - \int_{\mathcal{Z}_{t^*}}^{\mathcal{Z}} \frac{2mL_{loc}c_gK}{\sqrt{1-c_g^2K^2}} d\mathcal{Z}', \quad (\text{C.5})$$

and note that the joint process $\{m(\mathcal{Z}), S(\mathcal{Z}), X(\mathcal{Z})\}_{\mathcal{Z} \geq \mathcal{Z}'}$ is Markovian, with infinitesimal generator

$$\begin{aligned}\tilde{\mathbb{G}}\psi(M, s, \chi) &= \lim_{\eta \rightarrow 0} \frac{1}{\eta} [E\{\psi(m(\mathcal{Z} + \eta), S(\mathcal{Z} + \eta), X(\mathcal{Z} + \eta)) | m(\mathcal{Z}) = M, S(\mathcal{Z}) = s, X(\mathcal{Z}) = \chi\} - \psi(M, s, \chi)] \\ &= \lim_{\eta \rightarrow 0} \frac{1}{\eta} \left\{ [\psi(M+1, s, \chi) + \psi(M-1, s, \chi)] M^2\eta + \psi\left(M, s - \frac{2\eta ML_{loc}}{c_g\sqrt{1-c_g^2K^2}}, \chi - \frac{2\eta ML_{loc}c_gK}{\sqrt{1-c_g^2K^2}}\right) \right. \\ &\quad \left. \times (1 - 2M^2\eta) + o(\eta) - \psi(M, s, \chi) \right\} \\ &= \left\{ \mathbb{G} - 2M \left[\frac{L_{loc}}{c_g\sqrt{1-c_g^2K^2}} \frac{\partial}{\partial s} + \frac{L_{loc}c_gK}{\sqrt{1-c_g^2K^2}} \frac{\partial}{\partial \chi} \right] \right\} \psi(M, s, \chi).\end{aligned}$$

The solution of (C.3) is given by the Feynman-Kac formula [17]

$$\begin{aligned}W_M(\omega, K, s, \chi, z(\mathcal{Z})) &= E\{W_{m(\mathcal{Z})}(\omega, K, S(\mathcal{Z}), X(\mathcal{Z}), \mathcal{Z}_{t^*}) | m(\mathcal{Z}_{t^*}) = M, S(\mathcal{Z}_{t^*}) = s, X(\mathcal{Z}_{t^*}) = \chi\} \\ &= E\left\{ \delta_{0, m(\mathcal{Z})} \delta \left[s - \int_{\mathcal{Z}_{t^*}}^{\mathcal{Z}} \frac{2mL_{loc}}{c_g\sqrt{1-c_g^2K^2}} d\mathcal{Z}' \right] \delta \left[\chi - \int_{\mathcal{Z}_{t^*}}^{\mathcal{Z}} \frac{2mL_{loc}c_gK}{\sqrt{1-c_g^2K^2}} d\mathcal{Z}' \right] \Big| m(\mathcal{Z}_{t^*}) = M \right\},\end{aligned}$$

and the result stated in Lemma 4.6 follows after returning to the depth variable z ,

$$W_M(\omega, K, s, \chi, z) = E_M \left\{ \delta_{0, m(\mathcal{Z}(z))} \delta \left[s - \int_{-\mathcal{L}_{t^*}}^z \frac{2m(\mathcal{Z}(z'))}{c\sqrt{1-c^2K^2}} dz' \right] \delta \left[\chi - \int_{-\mathcal{L}_{t^*}}^z \frac{2m(\mathcal{Z}(z'))cK}{\sqrt{1-c^2K^2}} dz' \right] \right\}. \quad (\text{C.6})$$

Here we used the short notation E_M for the expectation conditioned by $m(\mathcal{Z}_{t^*}) = M$.

C.1. Homogeneous background. In the case $c(z) = c_o$, (C.6) simplifies to

$$W_M(\omega, K, s, \chi, z) = E_M \left\{ \delta_{0, m(\mathcal{Z}(z))} \delta \left[s - \frac{2}{c_o\sqrt{1-c_o^2K^2}} \int_{-\mathcal{L}_{t^*}}^z m(\mathcal{Z}(z')) dz' \right] \right\} \delta [\chi - Kc_o^2s], \quad (\text{C.7})$$

as we remarked in section 4.5. We are interested in evaluating W_M at the surface $z = 0$. As we explained in section 4.5, $W_M(\omega, K, s, \chi, 0)$ is not affected by the precise choice of t^* , as long as we observe it at times s that are smaller than t^* . This means that we may let $t^* \rightarrow \infty$ or, equivalently, $\mathcal{L}_{t^*} \rightarrow \infty$ and $\mathcal{Z}_{t^*} \rightarrow -\infty$.

To take the limit, it is convenient to shift coordinates and introduce a new process

$$\tilde{m}(\xi) = m(\mathcal{Z}_{t^*} + \xi), \quad \xi \in [0, -\mathcal{Z}_{t^*}], \quad (\text{C.8})$$

where

$$\xi(z) = \mathcal{Z}(z) - \mathcal{Z}_{t^*} = \int_{-\mathcal{L}_{t^*}}^z \frac{dz'}{L_{loc}(\omega, c_o, z')} = \frac{\omega^2 l}{4c_o^2(1 - c_o^2 K^2)}(z + \mathcal{L}_{t^*}), \quad -\mathcal{L}_{t^*} < z < 0. \quad (\text{C.9})$$

The new process satisfies the boundary conditions

$$\tilde{m}(0) = m(\mathcal{Z}_{t^*}) = M \quad \text{and} \quad \tilde{m}(-\mathcal{Z}_{t^*}) = m(0) \quad (\text{C.10})$$

and we use it to define the random variable

$$\nu_M^{t^*} = \frac{2}{c_o \sqrt{1 - c_o^2 K^2}} \int_{-\mathcal{L}_{t^*}}^0 m(\mathcal{Z}(z')) dz' = \frac{2}{c_o \sqrt{1 - c_o^2 K^2}} \int_{-\mathcal{L}_{t^*}}^0 \tilde{m}(\xi(z')) dz'. \quad (\text{C.11})$$

Now we can let $t^* \rightarrow \infty$, so that ξ is in the half space $[0, \infty)$. The process $\{\tilde{m}(\xi)\}_{\xi \geq 0}$ is recurrent [27], which means that $\tilde{m}(\xi)$ always reaches the absorbing state 0 for some bounded, (random) value of ξ . Thus, (C.11) has a limit

$$\nu_M = \lim_{t^* \rightarrow \infty} \nu_M^{t^*}, \quad (\text{C.12})$$

and $W_M(\omega, K, s, \chi, 0)$ is given by

$$W_M(\omega, K, s, \chi, 0) = E \{ \delta[s - \nu_M] | \tilde{m}(0) = M \} \delta[\chi - Kc_o^2 s]. \quad (\text{C.13})$$

It remains to compute

$$f_{\nu_M}(s) = E \{ \delta[s - \nu_M] | \tilde{m}(0) = M \}, \quad (\text{C.14})$$

the probability density function of ν_M .

The density $f_{\nu_M}(s)$ can be obtained as follows. We note that we need only the process $S(\xi)$, which is basically the same as that in (C.5), except that it depends on the shifted coordinate ξ . To avoid singularities, we compute first the cumulative distribution $\mathcal{F}_{\nu_M}(s) = \int_0^s f_{\nu_M}(t) dt$, which satisfies

$$\begin{aligned} \frac{2ML_{loc}}{c_o \sqrt{1 - c_o^2 K^2}} \frac{\partial \mathcal{F}_{\nu_M}}{\partial s} &= M^2 (\mathcal{F}_{\nu_{M+1}} - 2\mathcal{F}_{\nu_M} + \mathcal{F}_{\nu_{M-1}}), \quad s > 0, \\ \mathcal{F}_{\nu_M}(0) &= \delta_{0,M}. \end{aligned} \quad (\text{C.15})$$

This simple equation can be solved explicitly, and we obtain

$$\mathcal{F}_{\nu_M}(s) = \left[\frac{\tilde{s}}{2 + \tilde{s}} \right]^M 1_{[0, \infty)}(s), \quad \tilde{s} = \frac{\omega^2 l s}{4c_o \sqrt{1 - c_o^2 K^2}}, \quad (\text{C.16})$$

where $1_{[0, \infty)}(s)$ is the Heaviside step function. The result

$$E \{ \delta[s - \nu_M] | m(0) = M \} = f_{\nu_M}(s) = \frac{\omega^2 l M}{2c_o \sqrt{1 - c_o^2 K^2}} \frac{\tilde{s}^{M-1}}{(2 + \tilde{s})^{M+1}} 1_{[0, \infty)}(s) \quad (\text{C.17})$$

follows from (C.13), after differentiating (C.16) with respect to s . Furthermore, we have from (C.12) and (C.17) that in the particular case $M = 1$,

$$W_1(\omega, K, s, \chi, 0) = \frac{\omega^2 l}{2c_o \sqrt{1 - c_o^2 K^2}} \frac{1_{[0, \infty)}(s)}{(2 + \bar{s})^2} \delta[\chi - Kc_o^2 s]. \quad (\text{C.18})$$

This is the formula used in the proof of Theorem 4.5.

REFERENCES

- [1] MARK ASCH, *Analysis and Numerical Solution of a Transport Equation for Pulse Reflection in a Randomly Layered Medium*, PhD thesis, New York University, June 1990.
- [2] M. ASCH, W. KOHLER, G. PAPANICOLAOU, M. POSTEL, AND B. WHITE, *Frequency content of randomly scattered signals*, SIAM Review, 33 (1991), pp. 519–625.
- [3] ———, *Statistical inversion from reflections of spherical waves by a randomly layered medium*, Waves in Random Media, 6 (1996), pp. 293–334.
- [4] E. BÉCACHE, P. JOLY, AND C. TSOGKA, *Etude d'un nouvel élément fini mixte permettant la condensation de masse*, C. R. Acad. Sci. Paris Sér. I Math., 324 (1997), pp. 1281–1286.
- [5] ———, *An analysis of new mixed finite elements for the approximation of wave propagation problems*, SIAM J. Numer. Anal., 37 (2000), pp. 1053–1084.
- [6] BIONDO BIONDI, *3D Seismic Imaging*, no. 14 in Investigations in Geophysics, Society of Exploration Geophysicists, Tulsa, 2006.
- [7] G. BLAKENSHIP AND G. PAPANICOLAOU, *Stability and control of systems with white-band noise disturbances*, SIAM J. Appl. Math., 34 (1978), pp. 437–476.
- [8] N. BLEISTEIN, J.K. COHEN, AND J.W. STOCKWELL JR., *Mathematics of multidimensional seismic imaging, migration, and inversion*, Springer, New York, 2001.
- [9] L. BORCEA, F. GONZÁLEZ DEL CUETO, G. PAPANICOLAOU, AND C. TSOGKA, *Data filtering for imaging in heavy clutter*, preprint to be submitted to Inverse Problems, (2008).
- [10] ———, *Filtering deterministic layer effects in imaging*, SIAM Multiscale Model. Simul., 7(3) (2009), pp. 1267–1301.
- [11] L. BORCEA, G. PAPANICOLAOU, AND C. TSOGKA, *Theory and applications of time reversal and interferometric imaging*, Inverse Problems, 19 (2003), pp. S139–S164. Special section on imaging.
- [12] ———, *Adaptive interferometric imaging in clutter and optimal illumination*, Inverse Problems, 22 (2006), pp. 1405–1436.
- [13] ———, *Coherent interferometric imaging in clutter*, Geophysics, 71 (2006), pp. 1165–1175.
- [14] ———, *Coherent interferometry in finely layered random media*, SIAM Multiscale Model. Simul., 5 (2006), pp. 62–83.
- [15] ———, *Asymptotics for the space-time Wigner transform with applications to imaging*, in Stochastic differential equations: theory and applications, Peter H. Baxendale and Sergey V. Lototsky, eds., vol. 2 (In honor of Prof. Boris L. Rozovskii) of Interdisciplinary Mathematical Sciences, World Scientific, 2007, pp. 91–112.
- [16] B. BORDEN, *Mathematical problems in radar inverse scattering*, Inverse Problems, 19 (2002), pp. R1–R28.
- [17] L. BREIMAN, *Probability*, SIAM, second printing ed., 1993.
- [18] R. BURRIDGE, G. PAPANICOLAOU, P. SHENG, AND B. WHITE, *Probing a random medium with a pulse*, SIAM J. Appl. Math., 49 (1989), pp. 582–607.
- [19] R. BURRIDGE, G. PAPANICOLAOU, AND B. WHITE, *One dimensional wave propagation in a highly discontinuous medium*, Wave Motion, 10 (1988), pp. 19–44.
- [20] J. CARAZZONE AND W. SYMES, *Velocity inversion by differential semblance optimization*, Geophysics, 56 (1991).
- [21] J. F. CLAERBOUT, *Fundamentals of geophysical data processing : with applications to petroleum prospecting*, CA : Blackwell Scientific Publications, Palo Alto, 1985.
- [22] J. F. CLAERBOUT, *Earth soundings analysis: Processing versus inversion*, Blackwell Scientific Publications, Inc., 1992.
- [23] J. F. CLOUET AND J. P. FOUQUE, *Spreading of a pulse travelling in random media*, Annals of Applied Probability, Vol.4, No.4, (1994).
- [24] J. F. CLOUET, J. P. FOUQUE, AND M. POSTEL, *Spectral analysis of randomly scattered signals using the wavelet transform*, Wave Motion, 22 (1995), pp. 145–170.
- [25] F. COLLINO, P. JOLY, AND F. MILLOT, *Perfectly matched absorbing layers for the paraxial equations*, J. Computational Physics, 131 (1996), pp. 164–180.
- [26] J.C. CURLANDER AND R.N. MCDONOUGH, *Synthetic Aperture Radar*, Wiley, New York, 1991.
- [27] W. FELLER, *An introduction to probability theory and its applications*, vol. 1, John Wiley & Sons, 3 ed., 1968.
- [28] S. FOMEL, *Application of plane-wave destruction filters*, Geophysics, 67 (2002), pp. 1946–1960.
- [29] S. FOMEL, E. LANDA, AND M. TURHAM TANER, *Poststack velocity analysis by separation and imaging of seismic diffractors*, Geophysics, 72 (2007), pp. U89–U94.
- [30] J.-P. FOUQUE, J. GARNIER, G. PAPANICOLAOU, AND K. SÖLNA, *Wave Propagation and Time Reversal in Randomly Layered Media*, Springer, April 2007.
- [31] R.F. O'DOHERTY AND N. A. ANSTEY, *Reflections on amplitudes*, Geophysical Prospecting, 19 (1971), pp. 430–458.
- [32] G. PAPANICOLAOU, D. W. STOOCK, AND S. R. S. VARADHAN, *Martingale approach to some limit theorems*, in Statistical Mechanics and Dynamical Systems, Duke turbulence conference, D. Ruelle, ed., Duke Univ. Math. Series III, part IV, 1976, pp. 1–120.

- [33] L. RYZHIK, G. PAPANICOLAOU, AND J. B. KELLER, *Transport equations for elastic and other waves in random media*, *Wave Motion*, 24 (1996), pp. 327–370.
- [34] P. SHENG, *Introduction to wave scattering, localization and mesoscopic phenomena*, Academic Press, 1995.
- [35] K. SØLNA AND G. PAPANICOLAOU, *Ray theory for a locally layered random medium*, *Waves Random Media*, (2000).
- [36] B. WHITE, P. SHENG, AND B. NAIR, *Localization and backscattering spectrum of seismic waves in stratified lithology*, *Geophysics*, (1990), pp. 1158–1165.